Towards the Improved Robustness of Acoustic Cooperative Localization

by

Janille M. Maragh

S.B., Massachusetts Institute of Technology (2013)

Submitted to the Department of Mechanical Engineering
in partial fulfillment of the requirements for the degree of

Master of Science in Mechanical Engineering

at the

MASSACHUSETTS INSTITUTE OF TECHNOLOGY

February 2016

Author ..... Signature redacted
Department of Mechanical Engineering
September 30, 2015

Certified by ..... Signature redacted
John J. Leonard
Samuel C. Collins Professor of Mechanical and Ocean Engineering
Thesis Supervisor

Accepted by ..... Signature redacted
Rohan Abeyaratne
Quentin Berg Professor of Mechanics
Chairman, Department Committee on Graduate Students

Towards the Improved Robustness of Acoustic Cooperative Localization

by

Janille M. Maragh

Submitted to the Department of Mechanical Engineering
on September 30, 2015, in partial fulfillment of the
requirements for the degree of
Master of Science in Mechanical Engineering

Abstract

In this thesis, the relationship between packet loss and the accuracy of an autonomous surface craft's trajectory estimate is explored. In experimental conditions, it is common to lose subframes of acoustic packets, or even entire packets during transmission. Since packets are often used to encode localization information of and range measurements to the sender, lost packets result in poorer navigation of the receiving vehicle. Trajectory estimates, computed using nonlinear least squares optimization, are computed for a variety of client node/server code configurations, and for a series of packet transmission success rates in one of those configurations. Though it is possible for a vehicle to receive some subset of the total number of frames in a packet, partial packets are not usable in current methods. This thesis proposes a method of preparing acoustic packets containing navigation information, so that each frame of a packet is independently useful to a receiver. It is shown in this work that in incorporating navigation information from partially received packets as well, a more accurate trajectory estimate of a non-GPS-aided vehicle is achieved.

Thesis Supervisor: John J. Leonard
Title: Samuel C. Collins Professor of Mechanical and Ocean Engineering

Acknowledgments

I would like to thank Professor John J. Leonard for his guidance since my time as an undergraduate, and for his abundant support through the completion of this thesis. I would also like to express special thanks to Dr. Liam Paull for always making an effort to help in my quest to find my identity as a graduate researcher, and to Dr. Michael Benjamin and Alon Yaari for introducing me to the exciting world of marine robotics at the very start of my graduate career. Furthermore, without the ample support from Josh Leighton with field experiments and the huge amount of work done by the Hovergroup in developing the autonomous kayaks, none of the work described in this thesis would be possible.

I would also like to thank my lab mates, Ted, Dave, Tom, Sudeep, Dehann, Ross and Mike, for always providing sound advice on navigating the world of research, listening ears in stressful times, and many much needed laughs over countless cups of coffee. Furthermore, my graduate experience thus far has been greatly enriched by a group of very special friends: Sara, Uyanga, Andrew, Mustafa, Connor, Katie, Tommaso, Claudio, Thao and Victor, thank you for being my biggest supporters in graduate school.

Most importantly, I would like to thank my parents and sister, for always being the most supportive people I've been so lucky to have in my life. Hundreds of Skype calls, boundless encouragement and many many cheers only begin to describe the reasons why my undergraduate and graduate years have been so much better because of you.

Contents

List of Figures

List of Tables

Chapter 1

Introduction

Over the past few decades, the world has seen a significant number of cases where autonomous underwater vehicles have been critical in searches and discoveries. Examples of Earth exploration in which autonomous underwater vehicles have been key include the discovery of the pink terraces in New Zealand [1] and general exploration of cavities under ice shelves in the Antarctic where globally important water mass transformations occur [2]. It has been noted that the techniques used for exploration on Earth, for example in Arctic exploration, could potentially be applied in extraterrestrial exploration [3].

More recently, with the loss of Malaysian Airlines flight MH370, the world has seen how important it is to deploy and execute missions in a time effective manner. The thirty-day lifetime of the batteries sustaining the black boxes aboard MH370 [4] is only one example in which efficient use of time is critical. Underwater vehicles also played a role in search and rescue initiatives in Japan after the 2011 Tōhoku earthquake and tsunami [5], and in investigations following the 2010 Deepwater Horizon oil spill [6] [7].

Missions involving vehicles on land or in the air generally have the advantage of being able to utilize GPS measurements continuously so that their pose (position, or position and orientation) is always known with acceptable certainty. However, since electromagnetic waves are rapidly attenuated by seawater, underwater vehicles cannot use GPS measurements to remain localized and must rely on other methods

to maintain an acceptable estimate of their pose. The combination of altimeters, which measure depth, compasses, which measure orientation, and velocity sensors, such as Doppler current profilers, allow for localization through velocity integration, or dead reckoning (DR), but due to measurement noise, the error of DR pose estimates inevitably grow without bound with time. Very expensive onboard sensors can slow the growth of DR error, but cannot eliminate the issue.

To counteract the unbounded grow of DR estimates, additional external measurements must be incorporated into a mission. An example of such an external measurement is a GPS fix, in which a vehicle surfaces to get access to a GPS measurement to reset its accumulated DR error. However, GPS fixes introduce extra time into a mission, and in addition to wasting energy, this may be impractical in time-sensitive cases, such as those mentioned above.

The long baseline acoustic positioning system (LBL) is one potential solution to this problem. Using the speed of sound in water, the time of flight of acoustic signals between vehicles and fixed beacons is used to compute the distance between them as described in equation 1.1, where v_{SW} is the speed of sound in seawater and $OWTT$ is the one-way travel time of the acoustic signal from the landmark beacon to the vehicle.

$$dist = v_{SW} \cdot OWTT \tag{1.1}$$

Since a vehicle's depth can be known with very high accuracy using low-cost pressure sensors, the localization using range problem becomes a planar problem. The ranges between a vehicle and three fixed beacons can be used to compute an unambiguous estimate of a vehicle's position, as shown in Figure 1-1.

A challenge of LBL systems, however, is that they reduce the working area of the autonomous vehicles to areas within a few kilometers of the fixed beacons [8]. In response to this challenge, the moving long baseline navigation (MLBL) method was proposed by Vaganay et al. [9], in which two unmanned surface vehicles (USVs) act as beacons, or communications and navigation aids (CNAs).

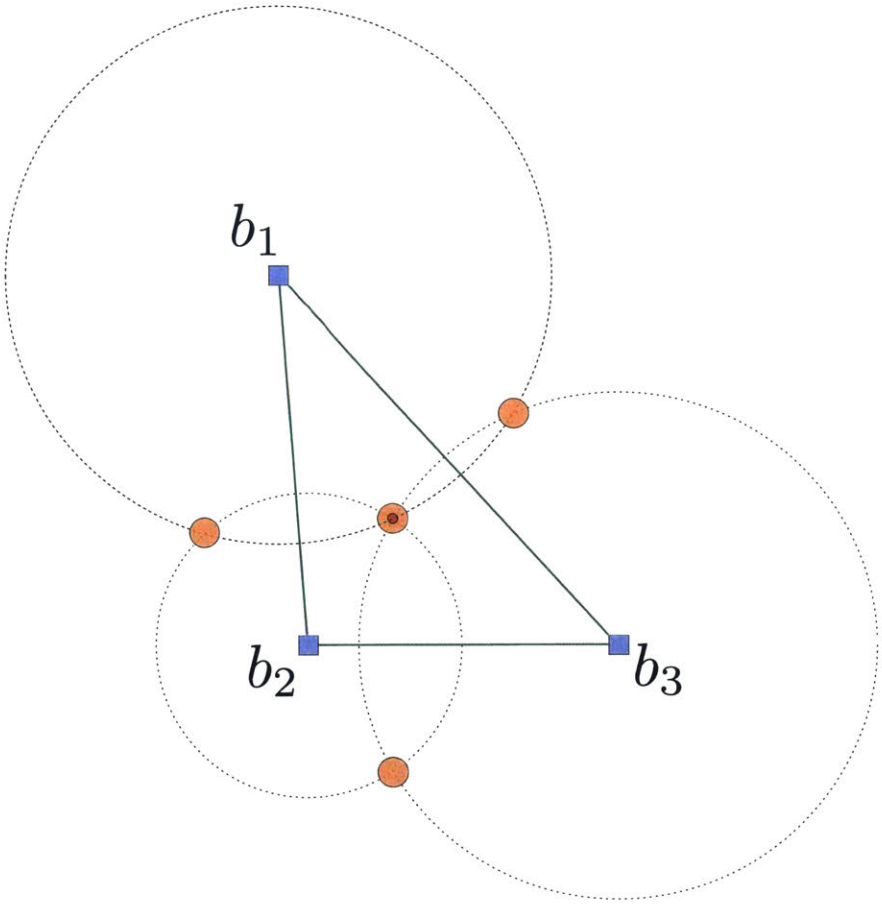

Figure 1-1: When range measurements to two beacons (purple squares) with access to GPS measurements are known, the set of possible positions of a vehicle of unknown position can be reduced to two possibilities on opposite sides of the baseline (solid green line) connecting the two beacons. If a range measurement to a third beacon is also known, the ambiguity is eliminated.

Other field experiments described in chapter 2 describe the extension of the MLBL, in which a range measurements to a single CNA are used to correct the DR error. In the problem of cooperative navigation, multiple AUVs use their own DR pose estimated and intervehicular ranges to significantly slow the growth of the localization error of each vehicle. The cooperative navigation problem relaxes the constraints of the previous cases, in that GPS-aided CNAs are not necessary.

1.1 Thesis Roadmap

The work in this thesis tackles a problem commonly encountered in field experiments. Acoustic packets containing localization estimates of vehicles, for example, are broadcast to other vehicles in a mission. Because of the scheme used to transmit acoustic packets, they are transmitted as sets of frames. As can be seen in Figure 1-2, it is common for packets to completely or partially be dropped. This is due to the numerous limitations presented by the acoustic environment. One major limitation is the attenuation of the acoustic signal due to the conversion of acoustic energy to heat, which increases with distance traveled. Reflection off the surface of the water or sea floor amplifies this problem, and multi-path also encourages distortion of the signal through interference with itself. The signal may also attenuate due to dispersion of the acoustic wave due to interaction with the turbulent ocean surface or the rough bathymetry of the sea floor. Furthermore, the signal also undergoes inverse-square law spherical geometric spreading; the intensity therefore decreases significantly the further the signal must travel [10]. These challenges make it difficult for acoustic packets to successfully reach their target receivers intact.

Whereas current methods functionally discard these partially received acoustic packets, this work describes how pose marginalization through spatial relationship compounding can be used to include low resolution information in each frame of an acoustic packet so that even when it is only partially successfully transmitted, an acoustic packet can still provide useful information to a target transducer for the purpose of cooperative localization. Details of this approach are described in Chapter

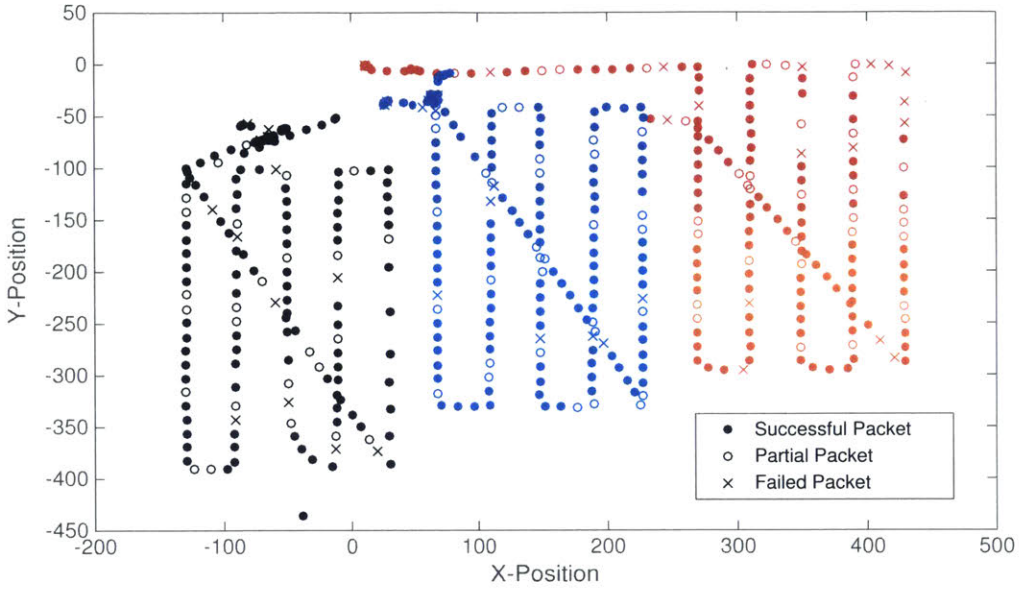

Figure 1-2: Figure showing packet success indicators superimposed on the GPS-measured trajectories of three vehicles on a mission executed on November 26th, 2014 on the Charles River in Cambridge, MA.

5.

Chapter 3 describes the sensor fusion maximum likelihood estimation (MLE) problem used to estimate a vehicle's trajectory for three different CNA-client node vehicle configurations, and for the case of two CNAs assisting one client node vehicle, the effect of packet loss on the nonlinear least square (NLS) trajectory estimate accuracy is explored. This method of computing the MLE of the client node's trajectory is strongly based on the work conducted by Eustice et al. in [11]. Chapter 4 describes the use of data from a three-vehicle mission, carried out on November 26th, 2014 by Dr. Liam Paull on the Charles River in Cambridge, MA, to determine the effect of partial packet loss on NLS trajectory estimate accuracy. Chapter 4 also describes the analysis of the error of that mission data and its use in estimating of the speed of sound in the water during the mission. Conclusions and topics for future work are included in Chapter 6.

Chapter 2

Literature Review

In recent years especially, strides have been made in the quality of the communication and navigation of ocean vehicles. In this chapter, the landscape of the field of the acoustic communication and cooperative navigation of autonomous underwater vehicles (AUVs) and autonomous surface crafts (ASCs) is described and discussed. A summary of the software used to obtain the data described later in the work is given, followed by a discussion of the state-of-the-art methods being used currently in acoustic cooperative navigation. Following that is an introduction to the pose graph representation of mission data, and a brief discussion of the state-of-the-art methods in state and trajectory estimation.

2.1 Relevant Software

The Mission Oriented Operating Suite-Interval Programming (MOOS-IvP) framework is the means of communication between deployed vehicles and the shoreside computer in the previously executed mission described in the results section of this thesis. The MOOS-IvP framework was designed at MIT in two stages. MOOS was developed at MIT by Dr. Paul Newman in 2001 as a method for coordinating communication between a number of applications. The IvP Helm was written as an extension of MOOS in 2004 by Dr. Mike Benjamin to coordinate vehicle behaviors using multi-objective optimization. [12]

MOOS is a publish-subscribe framework: each application subscribes to a set of variables, and using the values of the variables at the time of subscription, performs some set of operations, then publishes a set of variables, which may be subscribed to by other MOOS applications within that community. Each vehicle in a vehicle network is home to a separate MOOS community, but vehicles are able to communicate with each other through other means, such as over wifi or using the acoustic channel.

The Goby Underwater Autonomy Project, hereafter referred to as Goby, was developed by Dr. Toby Schneider at MIT to enable the seamless integration of multiple types of communication, from acoustic to wifi to serial to ethernet. The set of modules created in the Goby Project include a set of MOOS applications that may be used to coordinate acoustic communication during the missions described in this work.

One MOOS application in particular, pAcommsHandler, plays an important role in the coordination of intervehicular acoustic communication. Whenever messages to be transmitted over the network are prepared, pAcommsHandler, queues them for transmission and as the driver for the acoustic modem, also coordinates the subsequent broadcasting of acoustic packets.

Data marshalling is handled using the Dynamic Compact Control Language (DCCL), also designed by Dr. Toby Schneider. The DCCL method of data encoding takes into consideration the unreliability of the acoustic channel, and as such, uses a modified arithmetic encoder to achieve compressions ratios of approximately 85% when compared to standard 32-bit integers. Thus, a relatively small number of bits are used to encode information, enabling more efficient use of the acoustic channel [13].

2.2 State-of-the-Art in AUV Navigation

In much of the previous work done in the field of acoustic communication of AUVs, algorithms are tested on unmanned surface vehicles (USVs). Using USVs for testing algorithms is highly preferable to using AUVs, because cost, risk, and complexity of experiments are all significantly reduced. Furthermore, since USVs have access to to GPS or real time kinematic (RTK) measurements, which are often taken to

Figure 2-1: Autonomous kayak on the Charles River in Cambridge, MA.

be "ground truth," assessing of the quality of localization estimates becomes simple. Platforms such as the low-cost Surface Craft for Oceanographic and Undersea Testing (SCOUT) [14], the Autonomous Coastal Exploration System (ACES) [15], and the autonomous kayaks developed by the Hovergroup at MIT (shown in Figure 2-1) are all examples of USVs that, when outfitted with acoustic transponders, can be used to simulate AUVs in the testing of acoustic navigation and localization algorithms. In the experiments described in this thesis, autonomous kayaks are used in place of AUVs when running missions.

As mentioned earlier, it is important for AUVs to utilize external measurements to counteract the boundlessly increasing localization error associated with unaided inertial measurement unit (IMU) and Doppler velocity log (DVL) navigation. In early forms of such implementation using the acoustic channel, referred to as long baseline (LBL) acoustic positioning, AUVs would send range "requests" to systems of fixed beacons after which the fixed beacons would "respond" with acoustic signals. The two-way travel time (TWTT) would be used to compute range measurements to the fixed beacons, and given an appropriate number of independent range measurements, the AUV would be able to determine an unambiguous estimate of its position. However, since vehicles had to request this information in turn, the rate of information

gain for navigation fixes would inversely scale with the number of AUVs. Furthermore, fixed LBL systems limit the range of AUV operation to only 5-10 km [16].

Later methods incorporated the use of synchronous clocks to form passive systems, which eliminated this scaling issue. Instead of the request-respond architecture, beacons of known position in the global frame would periodically broadcast acoustic signals over the entire AUV network. Passively "listening" AUVs would then be able to incorporate range measurements to these beacons, computed using the speed of sound and the one-way travel time of the signals, into their own localization estimation problem.

Eustice et al. were among the first to use this type of system. In 2006, results were presented for a two node configuration: one surface vehicle (a ship) with continuous access to GPS measurements, which was in scheduled communication with a second submerged vehicle equipped with a DVL [17], [18]. In these experiments, the AUV received pseudo-range measurements (in the form of one-way travel times) to the GPS-aided ship and packets containing position data of the ship. Papadopulous et al. presented the results of an observability analysis of a system, consisting of a single USV acting as a CNA for one or more AUVs, which showed that using nonlinear least squares optimization was the best approach for using range and proprioceptive measurements to compute vehicle trajectories, compared to the EKF, the particle filter and the current point nonlinear least squares estimator [19]. Using a sensor fusion framework, Eustice et al. used nonlinear least squares optimization (Levenberg-Marquardt, in particular), to solve for the maximum likelihood estimate of each vehicle's trajectory in field experiments involving a GPS-aided ship, acting as a CNA for a Doppler-aided AUV [11]. Results of these experiments showed significant improvement over purely DR trajectory estimates.

Webster et al. presented results of the first deep water evaluation of this type of system by conducting similar experiments in 2009. A GPS-equipped ship was used as a CNA for a pressure depth sensor-, gyrocompass- and DVL-equipped AUV in the southern Mid-Atlantic Ridge, which had the goal of locating and mapping hydrothermal vents in depths of about 4km. These experiments highlighted the increased

length scales possible with synchronous clock-assisted navigation. Though the AUV was renavigated in post-processing, methods for online navigation were presented [20]. Further enabling the use of acoustic communication between any combination of fixed beacons, USVs and AUVs, Webster et al. developed a platform-independent acoustic communication and navigation system, which included host computers, acoustic modems, precision clocks and software which handled modem configuration, acoustic signal traffic and interfacing between the clocks and modems. [16].

Kalman filtering is a state estimation method which involves the use of a process model to predict the state and error covariance of a system, and the use of measurements to subsequently update that prediction. While Kalman filtering is acceptable for linear systems, the extended Kalman filter linearizes about points of interest and is therefore acceptable for nonlinear systems, such as trajectory estimation using range measurements. Kalman filters and information filters serve the same purpose, but when using the information filter, the inverse error covariance is tracked instead of the error covariance [21].

Webster et al. presented in 2012 a centralized extended Kalman filter (CEKF) approach to solving for the trajectories of both a GPS-aided ship and a proprioceptive sensor-outfitted AUV. In the CEKF method employed here, the state of the system consisted of both the trajectory of the ship and the trajectory of the AUV. State estimation was carried out in post processing, where the initial "guesses" of the trajectories were the maximum likelihood estimates computed using the method previously reported by Eustice et al. in [11]. In experiments carried out in 4km of water on the southern Mid-Atlantic Ridge, LBL methods were used to determine "ground truth." Experimental results of the CEKF implementation showed significant improvement in both the localization estimate of the AUV and the spatial uncertainty of the estimate when compared to DR estimates. [22]

Bahr et al. conducted experiments showing successful cooperative navigation of AUVs using an assortment of vehicles. In one experiment, two autonomous surface crafts (ASCs) were used as CNAs in the trajectory estimation of a third ASC. Further experiments conducted included the use of two ASCs as CNAs for localizing an

underwater glider, and the use of two ASCs as CNAs for localizing a Bluefin12 AUV [23]. The cooperative navigation algorithm presented by Bahr et al. addressed an important weakness of the EKF. By incorporating a large number of historical range measurements into each computation of a state estimate, the system was more robust to outlier range measurements and could recover more quickly in the time step following an outlier measurement. Another important takeaway from these experiments is the disadvantage of the request and answer architecture for acoustic communication; due to the lossy nature of the acoustic channel, some subset of requests were lost, and some subset of the answers to those requests were also lost. The result was a low measurement update frequency, which could be addressed by using a passive network of broadcasting and "listening" vehicles with synchronous clocks.

As AUVs became less expensive, it became more reasonable to deploy networks of multiple low cost vehicles for the collection of data over large areas, in which it would be too risky and time-intensive to deploy a single vehicle outfitted with expensive sensors. In using larger networks of AUVs with lower cost sensors, however, it becomes difficult to implement a centralized state estimator over the entire network. In 2013, Webster et al. presented work which showed that a decentralized extended information filter (DEIF) produces an identical estimate of the current state of a system as a centralized extended information filter (CEIF). In a decentralized system, vehicles (or nodes) of a network maintain their own state estimate using their proprioceptive sensors and intermittent external measurements. An advantage of using a decentralized approach to state estimation is that it is more easily extensible to larger networks of AUVs. Furthermore, whereas the centralized ematimator can only be implemented in the post-processing of mission data, decentralized estimators may be implemented in real time [24]. Experimental results for the DEIF in two cases were presented: a node pair of a server node with continuous access to GPS and a client node, which remained submerged; and a node pair of a server node with intermittent access to GPS and a client node, which remained submerged [25]. The results of the DEIF algorithm exactly replicated the results of the CEKF algorithm presented in [22], which was used as a benchmark in testing the DEIF algorithm [26]. The only

differences in estimation results between the two were linearization errors [27]. In the discussion of these experiments, the difficulty of handling the lossy nature of the acoustic communication channel was highlighted.

Walls et al. proposed in [28], [29] a method of addressing this problem by improving robustness to packet loss, dubbed the origin state method. It was noted in this work that it is impractical to send odometry measurements relative to a previously transmitted pose estimate. By sending composed odometry measurements relative to some predetermined origin, odometry information can robustly be shared over a network of vehicles. In the proposed method, each client node in a network passively "listens" for acoustic messages from a server node; these acoustic messages contain the pose of the server node relative to an origin state known by each client. Each time a message is received by a client node, a new pose can be added to a client-side pose graph of the server node by decompounding the existing client-side pose graph from the compounded origin-state pose.

Until this point, the previous work described has involved the localization of a single client node with the aid of one or more server nodes or CNAs. A more desirable case would involve the the localization of multiple AUVs or client nodes. A potential issue that arises when multiple vehicles share state and range information is the generation of inconsistent estimates. When a vehicle uses range measurements more than once, its state estimates become overconfident and in addition to making data association and outlier rejection more difficult, it significantly decreases the likelihood of converging on the correct state estimate. Bahr et al. showed in 2009 that in executing careful bookkeeping of the sources of measurements, re-use of range measurements can be avoided and estimates can be guaranteed to be consistent [30].

This method, though effective, proved to not scale well when used for a network of more than three or four vehicles, since the error covariance matrices that had to be transmitted among all vehicles would be too large, especially given the low throughput of the acoustic channel. In response to this problem, Fallon et al. proposed a framework which allowed for consistent and accurate cooperative navigation in a network of any number of AUVs. A database containing intervehicle ranges between

all vehicles and DR measurements of all vehicles is maintained on each vehicle, and only when a complete set of data is received, will a vehicle perform state estimation [31].

Paull et al. and Walls et al. have both presented decentralized methods of estimating the trajectory of multiple AUVs using communication methods robust to packet loss. In [32], Paull et al. demonstrated the use of factor composition and careful bookkeeping to robustly broadcast odometry measurements. Onboard each vehicle is a pose graph, which consists of the vehicle's own pose for all time as well as the poses of other vehicles in the network corresponding with each received message. Through the use of acknowledgement bits, confirmed incoming and outgoing "contact points" are determined, in which a "contact point" is the most recent instance at which successful communication occurred. By tracking these contact points, odometry measurements relative to these times are generated using a compounding operation before being transmitted. Thus, received odometry measurements can be correctly appended to the local pose graph of each vehicle, on which a smoothing approach is taken to estimate the vehicle's trajectory.

In the approach outlined by Walls et al. in [33], instead of transmitting individual poses to be added to the local factor graph of a receiving vehicle, poses are transmitted as in the origin state method over the network. First, factor composition is used to generate approximation of the vehicle's own chain (factor graph consisting of only binary odometry factors and unary prior factors, such as GPS measurements), then factor composition is utilized again to generate a the pose of a vehicle at the time of launch (TOL) of a message. When a vehicle receives an acoustic message, it then employs decomposition to reconstruct a relative odometry measurement using the odometry factors already received to add to its own pose graph. Since the origin state method is used when transmitting poses, every message can be used independently by a receiving vehicle, so acknowledgement bits are not needed.

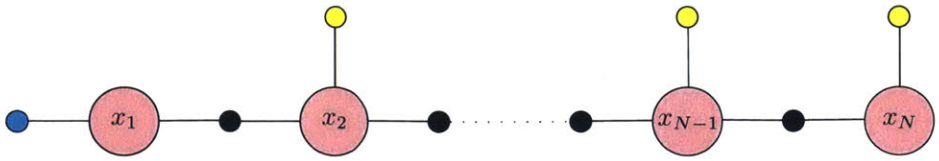

Figure 2-2: Example of a factor graph of a single vehicle. Shaded pink circles represent the nodes, or poses, of the vehicle, shaded black circles represent odometry measurements, and yellow circles represent priors, for example GPS fixes, which only apply to the poses to which they are connected. The blue shaded circle encodes the prior knowledge about the initial pose.

2.3 Algorithms for Trajectory Estimation

The factor graph, or pose graph, of a vehicle, as its name suggests, is a factorization of the function used to estimate its trajectory over the course of a mission, which is graphically represented as a bipartite graph. The graph consists of variable nodes (which represent vehicle poses in the work described here), and edges, which may be one of two types:

1. unary factors, which represent prior measurements, such as GPS fixes, and
2. binary factors, which represent spatial relationships between two successive poses, usually odometry measurements in the work described here.

Figure 2-2 shows an example of a vehicle's factor graph. Throughout the mission of this particular vehicle, the vehicle has the set of N poses $\boldsymbol{X} = [\boldsymbol{x}_1, ..., \boldsymbol{x}_N]$. It has some belief on its initial pose, and at each pose, the vehicle has access to an external measurement. A vehicle with an initial belief on its initial pose and continuous access to GPS measurements could have such a pose graph. Note that such a system is over-constrained; a least squares minimization approach could be applied, for example, to solve for the set of poses or the trajectory of the vehicle over the course of this mission.

As previously described, the error in the DR estimate of an AUV's pose will grow without bound with time in the absence of external measurements. Range and bearing measurements to landmarks may be incorporated into the pose graph of a vehicle, as shown in Figure 2-3 below. A landmark is an object in the vehicle's environment, which may be observed at multiple times (and therefore at multiple poses) throughout

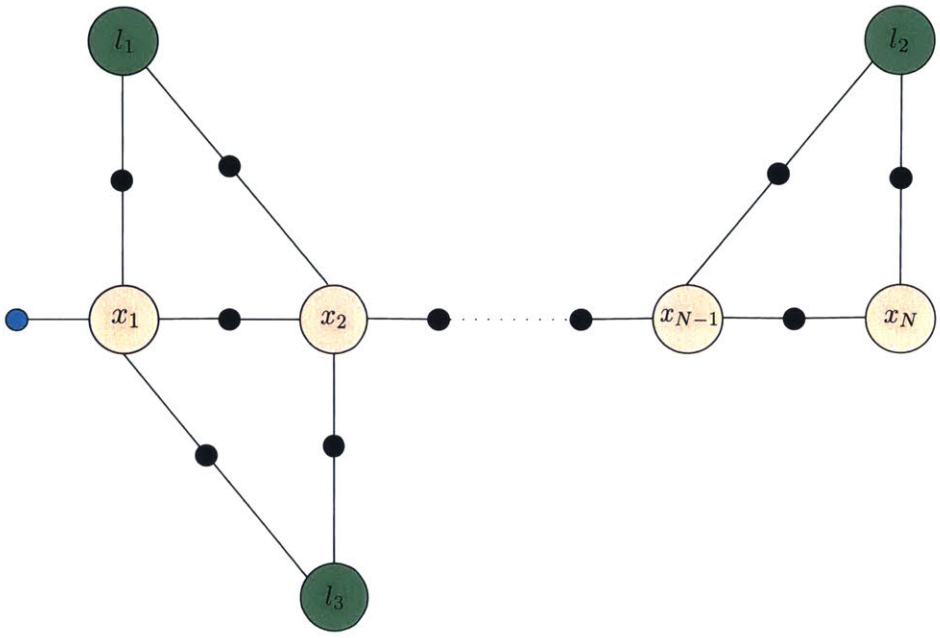

Figure 2-3: Factor graph of a single vehicle (pink shaded circles) with a prior on its initial pose, odometry measurements and measurements to three landmarks (shaded green circles).

a mission.

Range measurements to other vehicles may also be used to put a bound on the error associated with the DR pose estimate, in which case the problem becomes cooperative localization. The implementation of this method described in this thesis is strongly based on the sensor fusion maximum likelihood estimation problem presented by Eustice et al. in [11].

An example of a cooperative localization factor graph is shown in Figure 2-4. Chains of poses of multiple vehicles can be connected via range measurements between poses on different vehicles. A least squares formulation of the information provided in that factor graph may be solved to obtain trajectory estimates of each of the three vehicles. The schematic in Figure 2-4 shows how this communication of information would occur. At time $t = 1$, vehicle 2 broadcasts its pose. At time $t = 2$, it gets an acoustic packet from vehicle 3; this packet is associated with a range measurement and pose information about vehicle 3. A the next time step, vehicle 2 receives a packet from vehicle 1, and at the following time step, vehicle 2 broadcasts its pose information again.

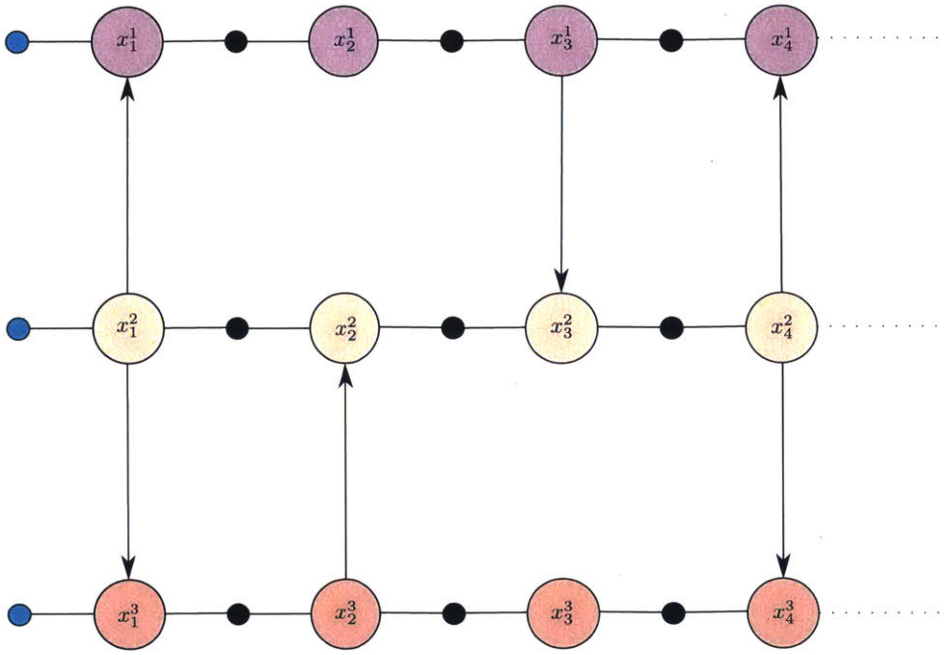

Figure 2-4: Schematic showing communication as experienced by center vehicle (pink variable nodes), which intermittently broadcasts its own localization estimate and is only aware of the state of the other two vehicles upon receipt of acoustic packets containing localization information of those vehicles.

Since there is inherent noise in each measurement, which is assumed to be zero-mean and normally distributed, each measurement only gives information about the vehicle's trajectory with a particular probability. For example, given the factor graph in Figure 2-2, the likelihood function for a set of poses i.e. a trajectory, $p(\boldsymbol{X}_i)$, is the joint distribution over the initial belief, $p(\boldsymbol{x}_0)$, and

1. the conditional probabilities that the $(N-1)$ odometry measurements, z_{odo} are made given consecutive poses, $\boldsymbol{x}_k$ and $\boldsymbol{x}_{k+1}$, and

2. the conditional probabilities that the N prior measurements are made given the vehicle's pose at time of measurement, $\boldsymbol{x}_k$

Therefore, the likelihood function of the trajectory estimate, where the set of all measurements is denoted as $\boldsymbol{Z}$ and the set of all poses is denoted as $\boldsymbol{X}$, is

$$p(\boldsymbol{Z}|\boldsymbol{X}) = p(\boldsymbol{x}_1) \prod_{i}^{N-1} p(\boldsymbol{z}_{odo_i}|\boldsymbol{x}_i, \boldsymbol{x}_{i+1}) \prod_{i}^{N} p(\boldsymbol{z}_{prior_i}|\boldsymbol{x}_i) \tag{2.1}$$

The maximum likelihood estimate (MLE) of the trajectory is thus

$$\hat{\boldsymbol{X}}_{ML} = \arg\max_{\boldsymbol{X}} p(\boldsymbol{Z}|\boldsymbol{X}) \tag{2.2}$$

which is equivalent to the minimization problem

$$\hat{\boldsymbol{X}}_{ML} = \arg\min_{\boldsymbol{X}} \; -\ln p(\boldsymbol{Z}|\boldsymbol{X}) \tag{2.3}$$

If the trajectory is taken to be a random variable, the maximum a posteriori (MAP) estimate of the trajectory may be computed. The MAP estimate is that trajectory which maximizes the posterior distribution on the estimate given the measurements obtained, that is

$$\hat{\boldsymbol{X}}_{MAP} = \arg\max_{\boldsymbol{X}} p(\boldsymbol{X}|\boldsymbol{Z}) \tag{2.4}$$

which is equivalent to the minimization problem

$$\hat{\boldsymbol{X}}_{MAP} = \arg\min_{\boldsymbol{X}} \; -\ln p(\boldsymbol{X}|\boldsymbol{Z}) \tag{2.5}$$

When the noise on the process model and the noise on the measurement model are zero-mean and normally distributed, as is assumed in this work, computing the MLE estimate or the MAP estimate becomes a nonlinear least squares problem [34]. Solving this nonlinear least squares problem for the MAP estimate of the entire trajectory is known as smoothing, as opposed to filtering, which makes a prediction for the kth pose estimate using the system's process model following the $(k-1)$th pose, which it updates once a measurement is taken. As a result, as mentioned before, smoothing approaches tend to be more robust to outlier measurements than filtering approaches. This least squares minimization problem can be solved using a number of iterative numerical solvers, such as the gradient descent method, the Gauss-Newton algorithm or the Levenberg-Marquardt algorithm, though more sophisticated methods for solving these problems have been developed in recent years.

Factor graphs like the ones described here result is what is known as a sparse least-squares problem, since most pose (i.e. variable) nodes are not directly connected to most other variable nodes in the factor graph. What results is a naturally sparse information matrix. Dellaert et al. presented a method, Square Root Smoothing and Mapping ($\sqrt{SAM}$) [34], which takes advantage of this natural sparsity to perform fast QR factorization of the information matrix to quickly solve for the trajectory of a vehicle.

In older methods, online pose estimation, such as in the case of online simultaneous mapping and localization (SLAM), was carried out by recomputing the entire trajectory as an independent problem each time a new factor was added to the factor graph (equivalent to adding a new summand to the least squares problem described above). Kaess et al. introduced the incremental smoothing and mapping (iSAM) algorithm, which took advantage of the sequential nature of the problem of online pose estimation by using new data to not recompute an entire new trajectory, but rather update the previous estimate of the trajectory. As opposed to older methods, which would re-execute the QR factorization of the entire information matrix upon the addition of every new pose, iSAM only updates the previous factorization by recomputing only the entries that change. Even when many landmark re-observations (i.e. loop closures) occur, the information matrix remains sparse since iSAM periodically reorders the variables to prevent the information matrix from becoming unnecessarily dense [35].

iSAM initially used the Gauss-Newton method to perform the least-squares minimization problem of trajectory estimation. The Gauss-Newton method is an iterative numerical method that uses an initial estimate and a number of quadratic approximations about that estimate and subsequent estimates to minimize a function to some predetermined satisfactory level. However, with the Gauss-Newton method, there is risk involved in that if a poor initial estimate is chosen for a significantly nonlinear problem, it is possible that an (incorrect) local minimum will be chosen as the solution to the problem.

Rosen et. al, in response to this issue, presented the Robust Incremental Least-Squares Estimation (RISE) approach, which is not only faster than the Gauss-Newton method for solving sparse least-squares problems, but also much more robust to this issue associated with significantly nonlinear least squares problems [36]. The RISE approach is now implemented iSAM.

2.4 Summary

In this chapter, the landscape of the field of acoustic communications-aided cooperative navigation and the state-of-the art methods in state and trajectory estimation were described. In the following chapter, the factor graph representation presented in this chapter is used to formulate the factorization of the maximum likelihood function of vehicles' trajectories. Nonlinear least squares optimization is then used to compute estimates of the vehicles' trajectories using simulated measurement data.

Chapter 3

Cooperative Localization Using Pose Graph Optimization

This chapter describes how the trajectories of client nodes may be solved for in a number of different experimental configurations, by generating a least squares formulation of the maximum likelihood equation for the trajectory estimates. Measurements from a number of different sensors are related to the trajectory variables, and a nonlinear least squares optimizer (here, the Levenberg-Marquardt algorithm) is used to solve for an estimate of the maximum likelihood trajectory. This method is very strongly based on the sensor fusion MLE problem presented by Eustice et al. in [11]. A least squares representation of the maximum likelihood estimate and the results of the optimization problem using simulated measurements are presented for the following cases.

1. Two client node vehicles, each with an initial GPS measurement, then noisy odometry measurements and noisy range measurements to a single CNA with access to GPS measurements thereafter.

2. Three vehicles, each with an initial GPS measurement, then only noisy odometry measurements and inter-vehicle range measurements thereafter.

3. A single client node vehicle with an initial GPS measurement, then noisy odometry measurements and noisy range measurements to two CNAs with access to

GPS measurements thereafter.

Using the ground truth (GPS) trajectory measurements of three vehicles from an actual mission, artificial range measurements and odometry measurements with added zero-mean, normally distributed noise were generated at regular time intervals and used to generate the trajectory estimates for the three vehicle configurations below.

3.1 State Description and Observation Models

In the presentation of the least squares problems to be solved, the state of a vehicle is fully described by its x- and y-coordinates in the global frame of the problem. The state vector for the ith vehicle in a mission is shown below.

$$\boldsymbol{x}_i(t) = [x_i(t), y_i(t)]^\top \equiv \boldsymbol{x}_i^k = [x_i^k, y_i^k]^\top \tag{3.1}$$

The index, k, is used to encode the inherent time dependence of the states of the vehicles. The states $\boldsymbol{x}_i^{k-1}$ and $\boldsymbol{x}_i^k$ represent consecutive states of the ith vehicle.

The GPS-derived observation model of the ith vehicle is defined as

$$\boldsymbol{z}_{GPS_i}^k = \boldsymbol{x}_i^k + \boldsymbol{w}_{GPS_i}^k \tag{3.2}$$

The term $\boldsymbol{w}_{GPS}^k$ represents the additive noise in the measurement; it is assumed to be zero-mean and normally distributed, with $\boldsymbol{w}_{GPS_i}^k \sim \mathcal{N}(0, \Sigma_{GPS_i}^k)$.

The vehicle-derived odometry measurement observation model for the ith vehicle is defined as

$$\boldsymbol{z}_{odo_i}^k = \boldsymbol{x}_i^k - \boldsymbol{x}_i^{k-1} + \boldsymbol{w}_{odo_i}^k \tag{3.3}$$

in which the term $\boldsymbol{w}_{odo,i}^k$ represents the additive noise in the measurement provided by the odometry sensor onboard the ith vehicle. It is assumed to be zero-mean and normally distributed with $\boldsymbol{w}_{odo,i}^k \sim \mathcal{N}(0, \Sigma_{odo,i}^k)$.

The inter-vehicle range between the ith and jth vehicle at the kth time-step is defined as

$$z^k_{r_{i,j}} = \| \boldsymbol{x}^k_i - \boldsymbol{x}^k_j \| + w^k_{r_{i,j}} \tag{3.4}$$

in which the term $w^k_{r_{i,j}}$ represents the additive noise in the range measurement, derived from the one-way travel time of the acoustic signal from the ith vehicle to the jth vehicle or vice versa. It is also assumed to be zero-mean and normally distributed with $w^k_{r_{i,j}} \sim \mathcal{N}(0, \Sigma^k_{r_{i,j}})$.

For all three cases described below, the odometry error covariances, based on the artificially added noise, were taken to be

$$\Sigma_{odo} = \begin{bmatrix} \sigma^2_{xx} & \sigma^2_{xy} \\ \sigma^2_{xy} & \sigma^2_{yy} \end{bmatrix} = \begin{bmatrix} 4 & 0 \\ 0 & 4 \end{bmatrix} \tag{3.5}$$

The range error covariance, based on the error analysis of the mission data, was taken to be

$$\Sigma_r = \sigma^2_r = 9 \tag{3.6}$$

And the error covariance of the GPS-measurements was estimated to be

$$\Sigma_{GPS} = \begin{bmatrix} \sigma^2_{xx} & \sigma^2_{xy} \\ \sigma^2_{xy} & \sigma^2_{yy} \end{bmatrix} = \begin{bmatrix} 0.01 & 0 \\ 0 & 0.01 \end{bmatrix} \tag{3.7}$$

3.2 Maximum Likelihood Estimation Problems

The maximum likelihood trajectory estimation problem is described in this section for the three vehicle configurations previously described. The objective function to be minimized in solving for the maximum likelihood trajectory estimate is presented along with the result of the optimization problem obtained using the Levenberg-Marquardt algorithm in conjunction with the artificial measurements.

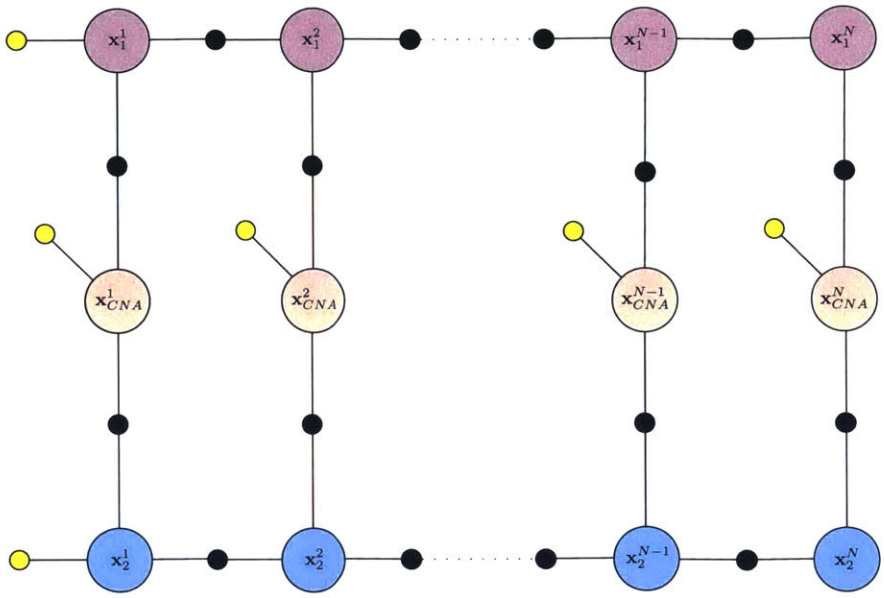

Figure 3-1: Pose graph of one CNA with access to GPS measurements (yellow shaded circles) assisting two client node vehicles (purple and red shaded circles). Binary factors connecting poses of different vehicles represent range-only measurements between vehicles. Binary factors connecting the poses of one of the client nodes represent odometry measurements.

3.2.1 One CNA Assisting Two Client Nodes

For the case of one CNA with access to GPS measurements assisting two client node vehicles, the problem is set up so that there are n time steps represented for each of the three vehicles. The CNA has access to n GPS measurements corresponding to its n poses, at times at which range measurements to each of the client nodes are made. Each client node vehicle also has access to $(n-1)$ odometry measurements, which in the field would come from its proprioceptive sensors. The pose graph for this configuration is shown in Figure 3-1, in which the CNA's poses are represented as pink shaded circles. The trajectories of the two client nodes are denoted as $\mathbf{X}_1 = \left[\mathbf{x}_1^1, ..., \mathbf{x}_1^N\right]$ and $\mathbf{X}_2 = \left[\mathbf{x}_2^1, ..., \mathbf{x}_2^N\right]$.

The sets of poses and measurements are defined as follows:

- The poses of the the CNA's trajectory:

$$\boldsymbol{X}_{CNA} = \left\{\boldsymbol{x}_{CNA}^k\right\}_0^{n-1} \tag{3.8}$$

- The poses of the first client node vehicle's trajectory:

$$\boldsymbol{X}_1 = \{\boldsymbol{x}_1^k\}_0^{n-1} \tag{3.9}$$

- The poses of the second client node vehicle's trajectory:

$$\boldsymbol{X}_2 = \{\boldsymbol{x}_2^k\}_0^{n-1} \tag{3.10}$$

- The GPS measurements of the CNA:

$$\boldsymbol{Z}_{GPS} = \{\boldsymbol{z}_{GPS}^k\}_0^{n-1} \tag{3.11}$$

- The odometry measurements of the first client node vehicle's trajectory:

$$\boldsymbol{Z}_{odo_1} = \{\boldsymbol{z}_{odo_1}^k\}_1^{n-1} \tag{3.12}$$

- The odometry measurements of the second client node vehicle's trajectory:

$$\boldsymbol{Z}_{odo_2} = \{\boldsymbol{z}_{odo_2}^k\}_1^{n-1} \tag{3.13}$$

- The inter-vehicle range measurements between the CNA and the first client node vehicle:

$$\boldsymbol{Z}_{r_1} = \left\{\boldsymbol{z}_{r_{1,CNA}}^k\right\}_0^{n-1} \tag{3.14}$$

- The inter-vehicle range measurements between the CNA and the second client node vehicle:

$$\boldsymbol{Z}_{r_2} = \left\{\boldsymbol{z}_{r_{2,CNA}}^k\right\}_0^{n-1} \tag{3.15}$$

All the poses form the variable $\boldsymbol{X}$ as

$$\boldsymbol{X} = \{\boldsymbol{X}_{CNA}, \boldsymbol{X}_1, \boldsymbol{X}_2\} \tag{3.16}$$

All the measurements form variable $\boldsymbol{Z}$ as

$$\boldsymbol{Z} = \{\boldsymbol{Z}_{GPS}, \boldsymbol{Z}_{odo_1}, \boldsymbol{Z}_{odo_2}, \boldsymbol{Z}_{r_1}, \boldsymbol{Z}_{r_2}\} \tag{3.17}$$

The maximum likelihood is thus

$$\hat{\boldsymbol{X}}_{ML} = \arg\max_{\boldsymbol{X}} p(\boldsymbol{Z}|\boldsymbol{X}) \tag{3.18}$$

which, when expanded, becomes

$$\begin{aligned}\hat{\boldsymbol{X}}_{ML} = \arg\max_{\boldsymbol{X}} & \, p(\boldsymbol{Z}_{GPS}|\boldsymbol{X}_{CNA}) p(\boldsymbol{Z}_{odo_1}|\boldsymbol{X}_1) \\ & p(\boldsymbol{Z}_{odo_2}|\boldsymbol{X}_2) p(\boldsymbol{Z}_{r_1}|\boldsymbol{X}_{CNA}, \boldsymbol{X}_1) p(\boldsymbol{Z}_{r_2}|\boldsymbol{X}_{CNA}, \boldsymbol{X}_2)\end{aligned} \tag{3.19}$$

This is converted to a least squared minimization problem as

$$\hat{\boldsymbol{X}}_{ML} = \arg\min_{\boldsymbol{X}} \; -\ln p(\boldsymbol{Z}|\boldsymbol{X}) \tag{3.20}$$

Using the previously defined observation models with additive, zero-mean, Gaussian noise, the nonlinear least squares minimization problem is written as

$$\begin{aligned}\hat{\boldsymbol{X}}_{ML} = \arg\max_{\boldsymbol{X}} & \frac{1}{2}\sum_{k=0}^{n-1}\left[\boldsymbol{z}^k_{r_{1,CNA}} - \parallel \boldsymbol{x}^k_1 - \boldsymbol{x}^k_{CNA} \parallel\right]^\top \left[\Sigma^k_{r_{1,CNA}}\right]^{-1} \left[\boldsymbol{z}^k_{r_{1,CNA}} - \parallel \boldsymbol{x}^k_1 - \boldsymbol{x}^k_{CNA} \parallel\right] \\ & + \frac{1}{2}\sum_{k=0}^{n-1}\left[\boldsymbol{z}^k_{r_{2,CNA}} - \parallel \boldsymbol{x}^k_2 - \boldsymbol{x}^k_{CNA} \parallel\right]^\top \left[\Sigma^k_{r_{2,CNA}}\right]^{-1} \left[\boldsymbol{z}^k_{r_{2,CNA}} - \parallel \boldsymbol{x}^k_2 - \boldsymbol{x}^k_{CNA} \parallel\right] \\ & + \frac{1}{2}\sum_{k=0}^{n-1}\left[\boldsymbol{z}^k_{GPS} - \boldsymbol{x}^k_{CNA}\right]^\top \left[\Sigma^k_{GPS}\right]^{-1} \left[\boldsymbol{z}^k_{GPS} - \boldsymbol{x}^k_{CNA}\right] \\ & + \frac{1}{2}\sum_{k=1}^{n-1}\left[\boldsymbol{z}^k_{odo_1} - \left(\boldsymbol{x}^k_1 - \boldsymbol{x}^{k-1}_1\right)\right]^\top \left[\Sigma^k_{odo_1}\right]^{-1} \left[\boldsymbol{z}^k_{odo_1} - \left(\boldsymbol{x}^k_1 - \boldsymbol{x}^{k-1}_1\right)\right] \\ & + \frac{1}{2}\sum_{k=1}^{n-1}\left[\boldsymbol{z}^k_{odo_2} - \left(\boldsymbol{x}^k_2 - \boldsymbol{x}^{k-1}_2\right)\right]^\top \left[\Sigma^k_{odo_2}\right]^{-1} \left[\boldsymbol{z}^k_{odo_2} - \left(\boldsymbol{x}^k_2 - \boldsymbol{x}^{k-1}_2\right)\right]\end{aligned} \tag{3.21}$$

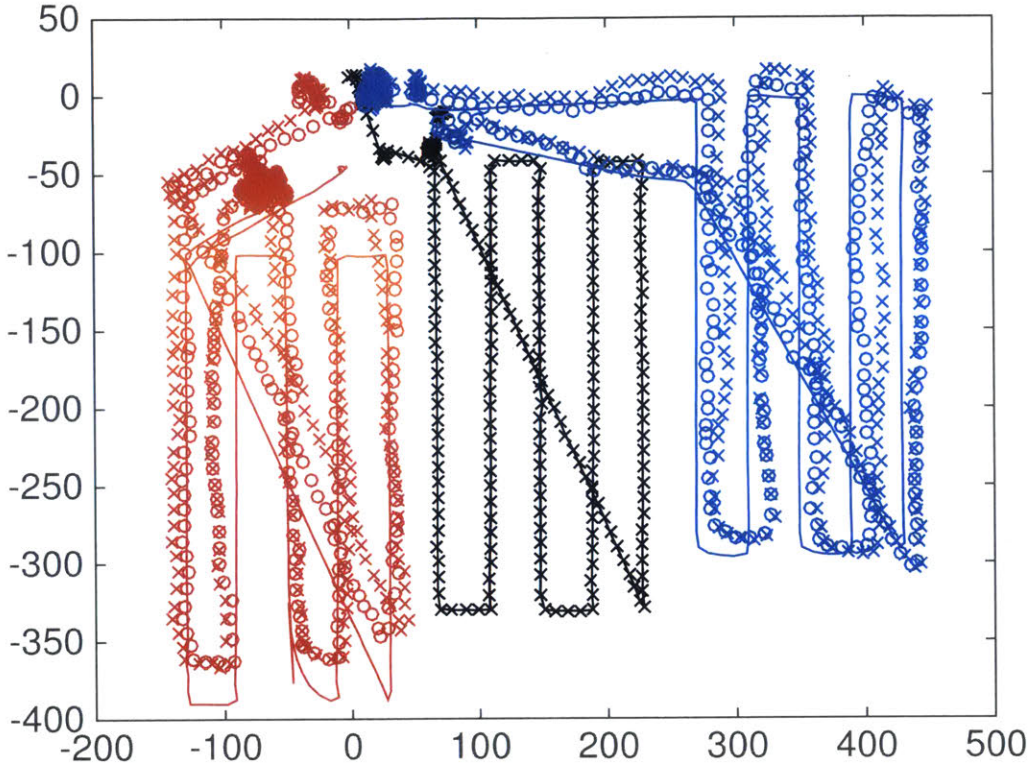

Figure 3-2: Results of NLS optimization of the trajectories of two vehicles, each with an initial GPS measurement, and odometry and inter-vehicle range measurements to a GPS-aided CNA (shown in black) thereafter. Ground truth as measured using GPS is shown with a solid line, dead-reckoned trajectory estimates are indicated with crosses, and NLS trajectory estimates are indicated with circles. Data of the same color indicates data for the same vehicle.

This nonlinear least squares minimization problem was solved using the MATLAB function, `lsqnonlin`, in conjunction with the artificial measurements. The result of the trajectory estimation problem for this configuration is shown below in Figure 3-2. The initial state estimate for the optimization problem was taken to be the dead-reckoned trajectory estimate of the two client node vehicles and the actual GPS-measured positions of the CNA.

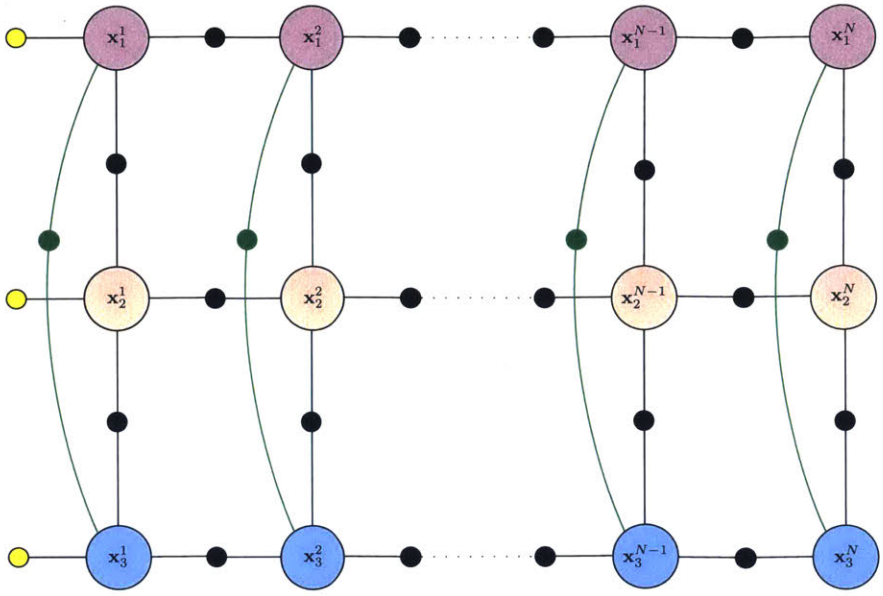

Figure 3-3: Pose graph of a three-vehicle network, each with an initial GPS measurement and none thereafter. Binary factors connecting poses of different vehicles represent the N range-only measurements between each pair of vehicles. For clarity, the binary factors indicating range measurements between vehicles 1 and 3 are colored green. Binary factors connecting the each vehicle's consecutive poses represent odometry measurements.

3.2.2 Trajectory Estimation of Three Vehicles Without CNAs

For the case in which there are no CNAs with access to GPS measurements throughout the mission, the problem is set up once again so that there are n time steps represented for each of the three vehicles. At each of each vehicle's n poses there are range measurements to each of other two vehicles in the mission. Each vehicle also has access to its $(n-1)$ odometry measurements. The pose graph for this configuration is shown in Figure 3-4. The trajectories of each of the three vehicles are denoted as $\mathbf{X}_1 = \left[\mathbf{x}_1^1, ..., \mathbf{x}_1^N\right]$, $\mathbf{X}_2 = \left[\mathbf{x}_2^1, ..., \mathbf{x}_2^N\right]$ and $\mathbf{X}_3 = \left[\mathbf{x}_3^1, ..., \mathbf{x}_3^N\right]$.

The sets of poses and measurements are defined as follows:

- The poses of the first vehicle's trajectory:

$$\boldsymbol{X}_1 = \left\{\boldsymbol{x}_1^k\right\}_0^{n-1} \tag{3.22}$$

- The poses of the second vehicle's trajectory:

$$\boldsymbol{X}_2 = \left\{\boldsymbol{x}_2^k\right\}_0^{n-1} \tag{3.23}$$

- The poses of the third vehicle's trajectory:

$$\boldsymbol{X}_3 = \left\{\boldsymbol{x}_3^k\right\}_0^{n-1} \tag{3.24}$$

- The odometry measurements of the first vehicle:

$$\boldsymbol{Z}_{odo_1} = \left\{\boldsymbol{z}_{odo_1}^k\right\}_1^{n-1} \tag{3.25}$$

- The odometry measurements of the second vehicle:

$$\boldsymbol{Z}_{odo_2} = \left\{\boldsymbol{z}_{odo_2}^k\right\}_1^{n-1} \tag{3.26}$$

- The odometry measurements of the third vehicle:

$$\boldsymbol{Z}_{odo_3} = \left\{\boldsymbol{z}_{odo_3}^k\right\}_1^{n-1} \tag{3.27}$$

- The inter-vehicle range measurements between first and second vehicles:

$$\boldsymbol{Z}_{r_{1,2}} = \left\{\boldsymbol{z}_{r_{1,2}}^k\right\}_0^{n-1} \tag{3.28}$$

- The inter-vehicle range measurements between first and third vehicles:

$$\boldsymbol{Z}_{r_{1,3}} = \left\{\boldsymbol{z}_{r_{1,3}}^k\right\}_0^{n-1} \tag{3.29}$$

- The inter-vehicle range measurements between second and third vehicles:

$$\boldsymbol{Z}_{r_{2,3}} = \left\{\boldsymbol{z}_{r_{2,3}}^k\right\}_0^{n-1} \tag{3.30}$$

All the poses form the variable $\boldsymbol{X}$ as

$$\boldsymbol{X} = \{\boldsymbol{X}_1, \boldsymbol{X}_2, \boldsymbol{X}_3\} \tag{3.31}$$

All the measurements form variable $\boldsymbol{Z}$ as

$$\boldsymbol{Z} = \left\{\boldsymbol{Z}_{odo_1}, \boldsymbol{Z}_{odo_2}, \boldsymbol{Z}_{odo_3}, \boldsymbol{Z}_{r_{1,2}}, \boldsymbol{Z}_{r_{1,3}}, \boldsymbol{Z}_{r_{2,3}}\right\} \tag{3.32}$$

The maximum likelihood is thus

$$\hat{\boldsymbol{X}}_{ML} = \arg\max_{\boldsymbol{X}} p(\boldsymbol{Z}|\boldsymbol{X}) \tag{3.33}$$

which, when expanded, becomes

$$\begin{aligned}\hat{\boldsymbol{X}}_{ML} = \arg\max_{\boldsymbol{X}} & \, p(\boldsymbol{Z}_{odo_1}|\boldsymbol{X}_1)p(\boldsymbol{Z}_{odo_2}|\boldsymbol{X}_2)p(\boldsymbol{Z}_{odo_3}|\boldsymbol{X}_3) \\ & p(\boldsymbol{Z}_{r_{1,2}}|\boldsymbol{X}_1, \boldsymbol{X}_2)p(\boldsymbol{Z}_{r_{1,3}}|\boldsymbol{X}_1, \boldsymbol{X}_3)p(\boldsymbol{Z}_{r_{2,3}}|\boldsymbol{X}_2, \boldsymbol{X}_3)\end{aligned} \tag{3.34}$$

This is converted to a least squared minimization problem as

$$\hat{\boldsymbol{X}}_{ML} = \arg\min_{\boldsymbol{X}} \; -\ln p(\boldsymbol{Z}|\boldsymbol{X}) \tag{3.35}$$

Using the previously defined observation models with additive, zero-mean, Gaussian noise, the nonlinear least squares minimization problem is written as

$$\hat{\boldsymbol{X}}_{ML} = \arg\max_{\boldsymbol{X}} \frac{1}{2}\sum_{k=0}^{n-1}\left[\boldsymbol{z}_{r_{1,2}}^{k} - \parallel \boldsymbol{x}_1^k - \boldsymbol{x}_2^k \parallel\right]^{\top}\left[\Sigma_{r_{1,2}}^{k}\right]^{-1}\left[\boldsymbol{z}_{r_{1,2}}^{k} - \parallel \boldsymbol{x}_1^k - \boldsymbol{x}_2^k \parallel\right]$$
$$+ \frac{1}{2}\sum_{k=0}^{n-1}\left[\boldsymbol{z}_{r_{1,3}}^{k} - \parallel \boldsymbol{x}_1^k - \boldsymbol{x}_3^k \parallel\right]^{\top}\left[\Sigma_{r_{1,3}}^{k}\right]^{-1}\left[\boldsymbol{z}_{r_{1,3}}^{k} - \parallel \boldsymbol{x}_1^k - \boldsymbol{x}_3^k \parallel\right]$$
$$+ \frac{1}{2}\sum_{k=0}^{n-1}\left[\boldsymbol{z}_{r_{2,3}}^{k} - \parallel \boldsymbol{x}_2^k - \boldsymbol{x}_3^k \parallel\right]^{\top}\left[\Sigma_{r_{2,3}}^{k}\right]^{-1}\left[\boldsymbol{z}_{r_{2,3}}^{k} - \parallel \boldsymbol{x}_2^k - \boldsymbol{x}_3^k \parallel\right]$$
$$+ \frac{1}{2}\sum_{k=1}^{n-1}\left[\boldsymbol{z}_{odo_1}^{k} - \left(\boldsymbol{x}_1^k - \boldsymbol{x}_1^{k-1}\right)\right]^{\top}\left[\Sigma_{odo_1}^{k}\right]^{-1}\left[\boldsymbol{z}_{odo_1}^{k} - \left(\boldsymbol{x}_1^k - \boldsymbol{x}_1^{k-1}\right)\right]$$
$$+ \frac{1}{2}\sum_{k=1}^{n-1}\left[\boldsymbol{z}_{odo_2}^{k} - \left(\boldsymbol{x}_2^k - \boldsymbol{x}_2^{k-1}\right)\right]^{\top}\left[\Sigma_{odo_2}^{k}\right]^{-1}\left[\boldsymbol{z}_{odo_2}^{k} - \left(\boldsymbol{x}_2^k - \boldsymbol{x}_2^{k-1}\right)\right]$$
$$+ \frac{1}{2}\sum_{k=1}^{n-1}\left[\boldsymbol{z}_{odo_3}^{k} - \left(\boldsymbol{x}_3^k - \boldsymbol{x}_3^{k-1}\right)\right]^{\top}\left[\Sigma_{odo_3}^{k}\right]^{-1}\left[\boldsymbol{z}_{odo_3}^{k} - \left(\boldsymbol{x}_3^k - \boldsymbol{x}_3^{k-1}\right)\right] \tag{3.36}$$

This nonlinear least squares minimization problem was solved using the MATLAB function, `lsqnonlin`, in conjunction with the artificial measurements. The resulting trajectory estimation problem for this case is shown below in Figure 3-4. The initial state estimate for the optimization problem was taken to be the dead-reckoned trajectory estimates of each of the three vehicles. Notably, the absence of any global positioning updates for any vehicles throughout the mission results in a somewhat poor estimate even after using nonlinear least squares optimization. However, Figure 3-5 shows that the overall NLS estimation error in the mission still remained lower than the overall dead-reckoned trajectory estimate error, particularly towards the end of the mission.

3.2.3 Two CNAs Assisting One Client Node

For the case of two CNAs with access to GPS measurements assisting one vehicle, the problem is set up so that there are n time steps represented for each of the three vehicles. For each of the CNAs, there are n GPS measurements, $(n-1)$ odometry

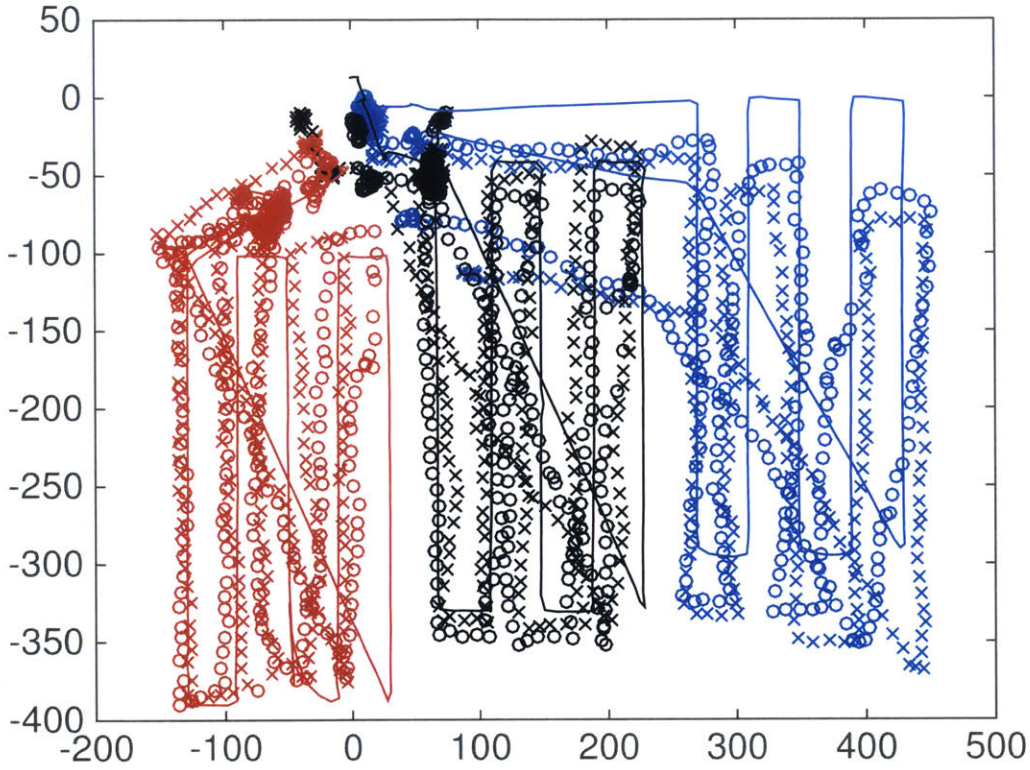

Figure 3-4: Results of NLS optimization of the trajectories of three vehicles each with an initial GPS measurement, and only odometry and inter-vehicle range measurements thereafter. Ground truth as measured using GPS is shown with a solid line, dead-reckoned trajectory estimates are indicated with crosses, and NLS trajectory estimates are indicated with circles. Data of the same color indicates data for the same vehicle.

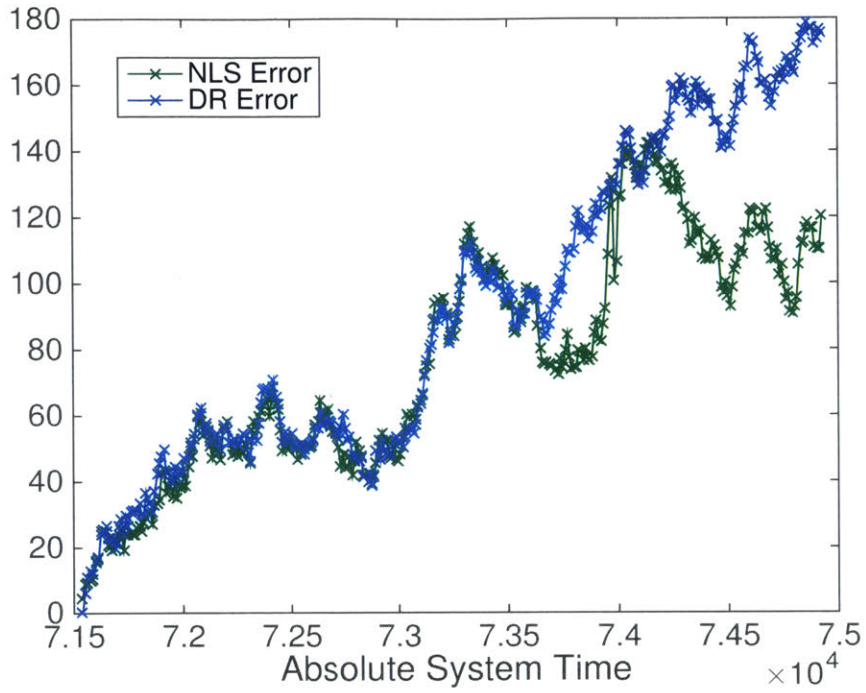

Figure 3-5: The sum of the NLS error and the DR error of all three vehicles over the course of the duration of the mission.

measurements for the vehicle without direct access to GPS measurements, and n OWTT-derived measured range measurements between the client node and each of the CNAs. The trajectory of the CNAs are denoted as $\mathbf{X}_1 = \left[\mathbf{x}_1^1, ..., \mathbf{x}_1^N\right]$ and $\mathbf{X}_2 = \left[\mathbf{x}_2^1, ..., \mathbf{x}_2^N\right]$ in the vehicle network's pose graph shown in Figure 3-6. The trajectory of the client node is denoted as $\mathbf{X}_u = \left[\mathbf{x}_u^1, ..., \mathbf{x}_u^N\right]$.

The sets of poses and measurements are defined as follows:

- The poses of the first CNAs trajectory:

$$\boldsymbol{X}_1 = \left\{\boldsymbol{x}_1^k\right\}_0^{n-1} \tag{3.37}$$

- The poses of the second CNAs trajectory:

$$\boldsymbol{X}_2 = \left\{\boldsymbol{x}_2^k\right\}_0^{n-1} \tag{3.38}$$

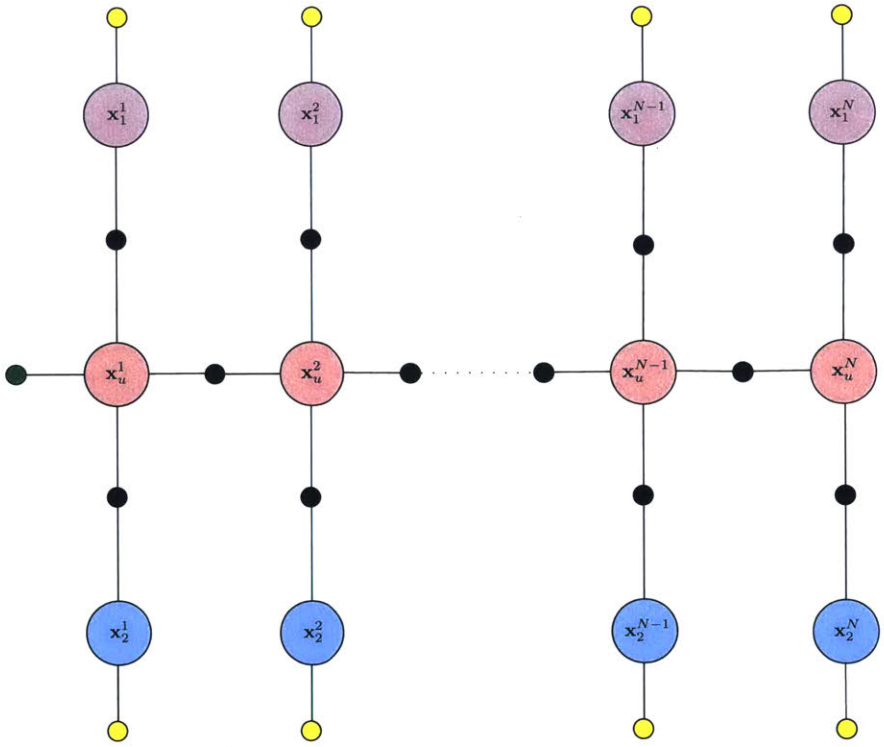

Figure 3-6: Pose graph of two CNAs with access to GPS measurements (yellow shaded circles) assisting one client node (pink shaded circles) with a single GPS measurement initialization (shaded green circle). Binary factors connecting poses of different vehicles represent range-only measurements between vehicles. Binary vehicles connecting the poses of the client node represent odometry measurements.

- The poses of the trajectory of "unknown" trajectory:

$$\boldsymbol{X}_u = \left\{\boldsymbol{x}_u^k\right\}_0^{n-1} \tag{3.39}$$

- The GPS measurements of the first CNA:

$$\boldsymbol{Z}_{GPS_1} = \left\{\boldsymbol{z}_{GPS_1}^k\right\}_0^{n-1} \tag{3.40}$$

- The GPS measurements of the second CNA:

$$\boldsymbol{Z}_{GPS_2} = \left\{\boldsymbol{z}_{GPS_2}^k\right\}_0^{n-1} \tag{3.41}$$

- The odometry measurements of the vehicle of "unknown" trajectory:

$$\boldsymbol{Z}_{odo_u} = \left\{\boldsymbol{z}_{odo_u}^k\right\}_1^{n-1} \tag{3.42}$$

- The inter-vehicle range measurements between the first CNA and the vehicle of "unknown" trajectory:

$$\boldsymbol{Z}_{r_1} = \left\{\boldsymbol{z}_{r_{1,u}}^k\right\}_0^{n-1} \tag{3.43}$$

- The inter-vehicle range measurements between the second CNA and the vehicle of "unknown" trajectory:

$$\boldsymbol{Z}_{r_2} = \left\{\boldsymbol{z}_{r_{2,u}}^k\right\}_0^{n-1} \tag{3.44}$$

All the poses form the variable $\boldsymbol{X}$ as

$$\boldsymbol{X} = \{\boldsymbol{X}_1, \boldsymbol{X}_2, \boldsymbol{X}_u\} \tag{3.45}$$

All the measurements form variable $\boldsymbol{Z}$ as

$$\boldsymbol{Z} = \left\{\boldsymbol{Z}_{GPS_1}, \boldsymbol{Z}_{GPS_2}, \boldsymbol{Z}_{odo_u}, \boldsymbol{Z}_{r_{1,u}}, \boldsymbol{Z}_{r_{2,u}}\right\} \tag{3.46}$$

The maximum likelihood is thus

$$\hat{\boldsymbol{X}}_{ML} = \arg\max_{\boldsymbol{X}} p(\boldsymbol{Z}|\boldsymbol{X}) \tag{3.47}$$

which, when expanded, becomes

$$\begin{aligned}\hat{\boldsymbol{X}}_{ML} = \arg\max_{\boldsymbol{X}} & \, p(\boldsymbol{Z}_{GPS_1}|\boldsymbol{X}_1)p(\boldsymbol{Z}_{GPS_2}|\boldsymbol{X}_2) \\ & p(\boldsymbol{Z}_{r_1}|\boldsymbol{X}_1, \boldsymbol{X}_u)p(\boldsymbol{Z}_{r_2}|\boldsymbol{X}_2, \boldsymbol{X}_u)p(\boldsymbol{Z}_{odo_1}|\boldsymbol{X}_u)\end{aligned} \tag{3.48}$$

This is converted to a nonlinear least squares minimization problem as

$$\hat{\boldsymbol{X}}_{ML} = \arg\min_{\boldsymbol{X}} \; -\ln p(\boldsymbol{Z}|\boldsymbol{X}) \tag{3.49}$$

Using the previously defined observation models with zero-mean, normally distributed additive noise, the nonlinear least squares minimization problem is stated as:

$$\begin{aligned}\hat{\boldsymbol{X}}_{ML} = \arg\max_{\boldsymbol{X}} & \frac{1}{2}\sum_{k=0}^{n-1}\left[\boldsymbol{z}^k_{r_{u,1}} - \parallel \boldsymbol{x}^k_u - \boldsymbol{x}^k_1 \parallel\right]^\top \left[\Sigma^k_{r_{u,1}}\right]^{-1}\left[\boldsymbol{z}^k_{r_{u,1}} - \parallel \boldsymbol{x}^k_u - \boldsymbol{x}^k_1 \parallel\right] \\ & + \frac{1}{2}\sum_{k=0}^{n-1}\left[\boldsymbol{z}^k_{r_{u,2}} - \parallel \boldsymbol{x}^k_u - \boldsymbol{x}^k_2 \parallel\right]^\top \left[\Sigma^k_{r_{u,2}}\right]^{-1}\left[\boldsymbol{z}^k_{r_{u,2}} - \parallel \boldsymbol{x}^k_u - \boldsymbol{x}^k_2 \parallel\right] \\ & + \frac{1}{2}\sum_{k=0}^{n-1}\left[\boldsymbol{z}^k_{GPS_1} - \boldsymbol{x}^k_1\right]^\top \left[\Sigma^k_{GPS_1}\right]^{-1}\left[\boldsymbol{z}^k_{GPS_1} - \boldsymbol{x}^k_1\right] \\ & + \frac{1}{2}\sum_{k=0}^{n-1}\left[\boldsymbol{z}^k_{GPS_2} - \boldsymbol{x}^k_2\right]^\top \left[\Sigma^k_{GPS_2}\right]^{-1}\left[\boldsymbol{z}^k_{GPS_2} - \boldsymbol{x}^k_2\right] \\ & + \frac{1}{2}\sum_{k=1}^{n-1}\left[\boldsymbol{z}^k_{odo_u} - \left(\boldsymbol{x}^k_u - \boldsymbol{x}^{k-1}_u\right)\right]^\top \left[\Sigma^k_{odo_u}\right]^{-1}\left[\boldsymbol{z}^k_{odo_u} - \left(\boldsymbol{x}^k_u - \boldsymbol{x}^{k-1}_u\right)\right]\end{aligned} \tag{3.50}$$

This nonlinear least squares minimization problem was solved using the MATLAB function, `lsqnonlin`, in conjunction with the artificial measurements. The resulting

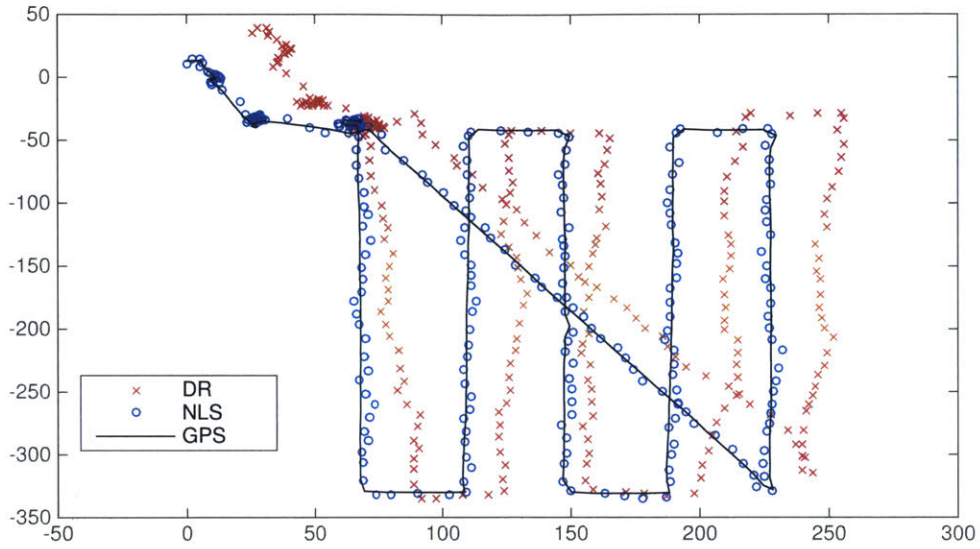

Figure 3-7: Results of NLS optimization of the trajectory a single client node vehicle with an initial GPS measurement, and only odometry and inter-vehicle range measurements to a GPS-aided CNA thereafter. Ground truth as measured using GPS is shown with a solid line, the dead-reckoned trajectory estimate of the vehicle is indicated using crosses, and the NLS trajectory estimate is indicated using circles.

trajectory estimate for this problem is shown below in Figure 3-7. The initial state estimate for the optimization problem was taken to be the dead-reckoned trajectory estimate of the client node and the actual GPS-measured positions of the two CNAs.

In this result, the assumption of a lossless channel was made, that is, all measurements were used. In the experimental equivalent under this assumption, every generated measurement (or sent acoustic packet) would be received by the intended target. However, the acoustic channel is far from lossless, and it is likely that some measurements would be dropped over the course of a mission. Here, the NLS trajectory estimate is recomputed for four cases: the 30%, 50%, 70% or 90% packet transmission success cases. Range measurements, and thus CNA GPS measurements as well, were artificially "lost" in the $N\%$ success case by randomly eliminating $(100 - N)\%$ of the generated measurements.

Figures 3-8, 3-9, 3-10 and 3-11 show the NLS trajectory estimate of the client node (circles), its dead-reckoned trajectory estimate (crosses) and its GPS-measured

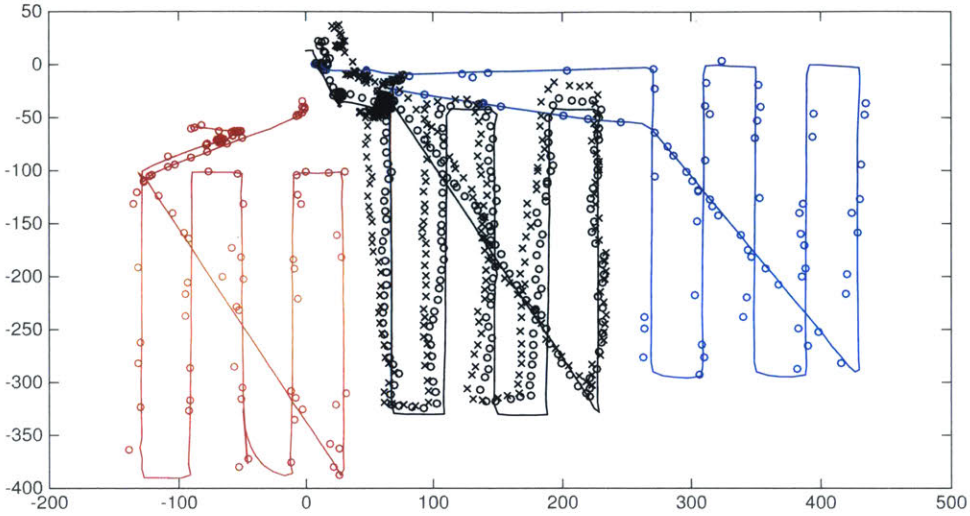

Figure 3-8: Maximum likelihood state estimation results with client node (black) using 30% of measurements from each CNA. Solid line: ground truth. Crosses: DR trajectory estimate. Circles: Maximum likelihood trajectory estimate.

trajectory (solid line), which was taken to be ground truth. It is apparent from the estimates that the quality of the trajectory estimate decreases as the proportion of packets lost increases.

Figure 3-12 shows the absolute spatial error in the NLS trajectory estimate with time, using the GPS-measured trajectory of the client node vehicle as ground truth. Throughout the mission, the NLS estimate of the client node's position remains in better agreement with ground truth in cases of higher packet transmission success rates.

In Figure 3-13, the quality of the NLS trajectory estimate is made more explicit for each of the four cases by showing the cumulative error in the trajectory estimate over the course of the mission.

3.3 The Levenberg-Marquardt Algorithm

The objective functions stated above for the various configurations of client nodes and CNAs were solved using the artificial measurements with the Levenberg-Marquardt

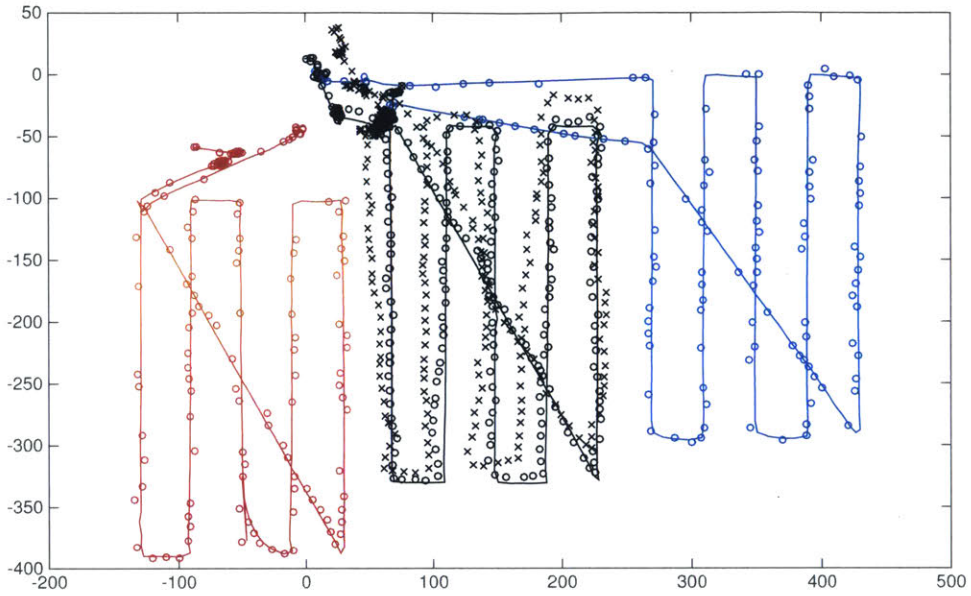

Figure 3-9: Maximum likelihood state estimation results with client node (black) using 50% of measurements from each CNA. Solid line: ground truth. Crosses: DR trajectory estimate. Circles: Maximum likelihood trajectory estimate.

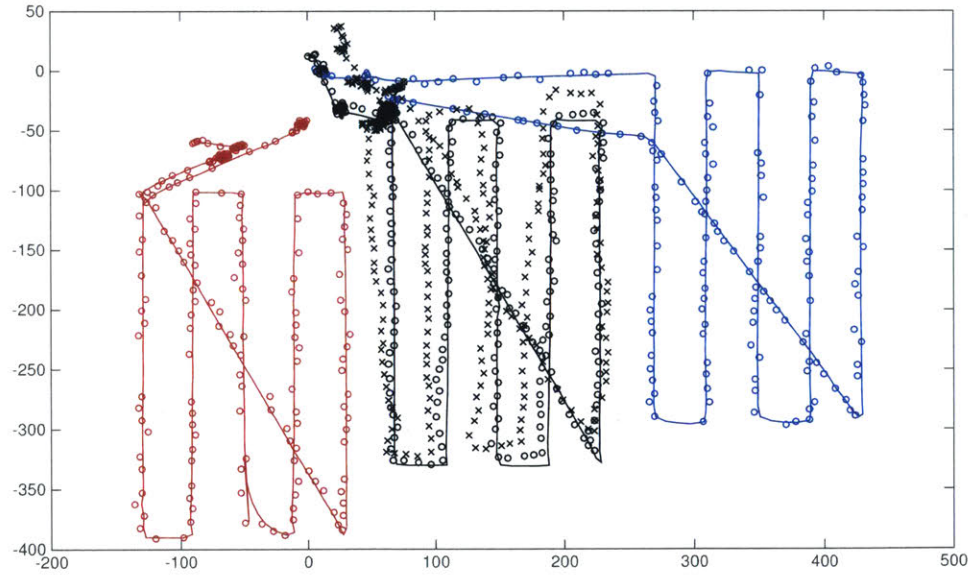

Figure 3-10: Maximum likelihood state estimation results with client node (black) using 70% of measurements from each CNA. Solid line: ground truth. Crosses: DR trajectory estimate. Circles: Maximum likelihood trajectory estimate.

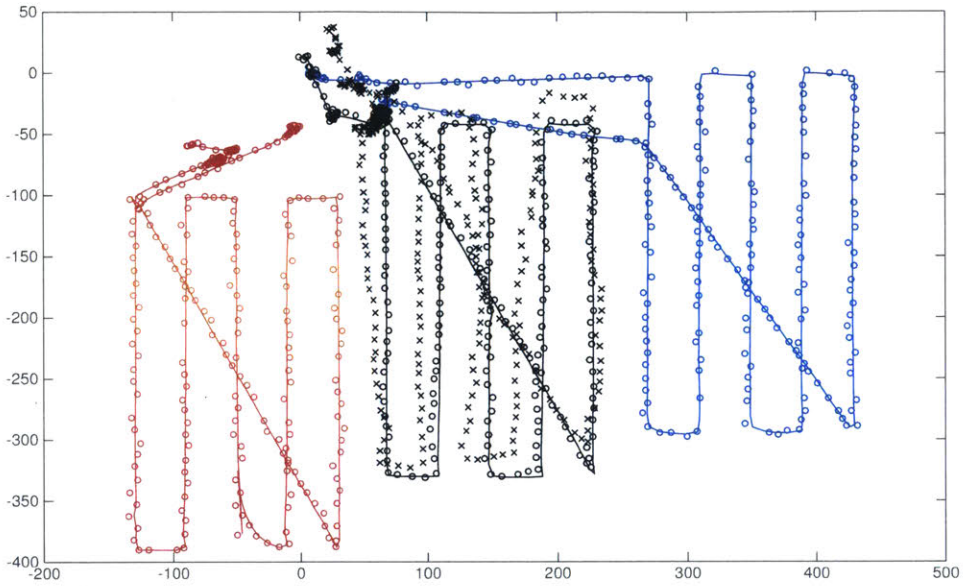

Figure 3-11: Maximum likelihood state estimation results with client node (black) using 90% of measurements from each CNA. Solid line: ground truth. Crosses: DR trajectory estimate. Circles: Maximum likelihood trajectory estimate.

algorithm, implemented in using the MATLAB function, `lsqnonlin`. The Levenberg-Marquardt method of minimizing an objective function involves the adaptive switching between two other iterative minimization methods: the gradient descent method and the Gauss-Newton method.

The gradient descent method starts with an initial belief of the state which minimizes the objective function. The gradient of the objective function is computed at this initial belief, and a step of size proportional to the magnitude of the gradient is taken in the direction opposite to the direction of the gradient. This is repeated until some stopping criterion is met. Though highly convergent, the gradient-descent method tends to perform more poorly near minima, since a large gradient near a minimum results in a larger step size, causing repeated overshooting of the minimum or "rattling out of the minimum" and thus slower convergence. [37]

The Gauss-Newton method shows better performance near minima by assuming that the function is approximately quadratic near the minimum and taking the curvature of the function into account. However, the gradient descent method has superior

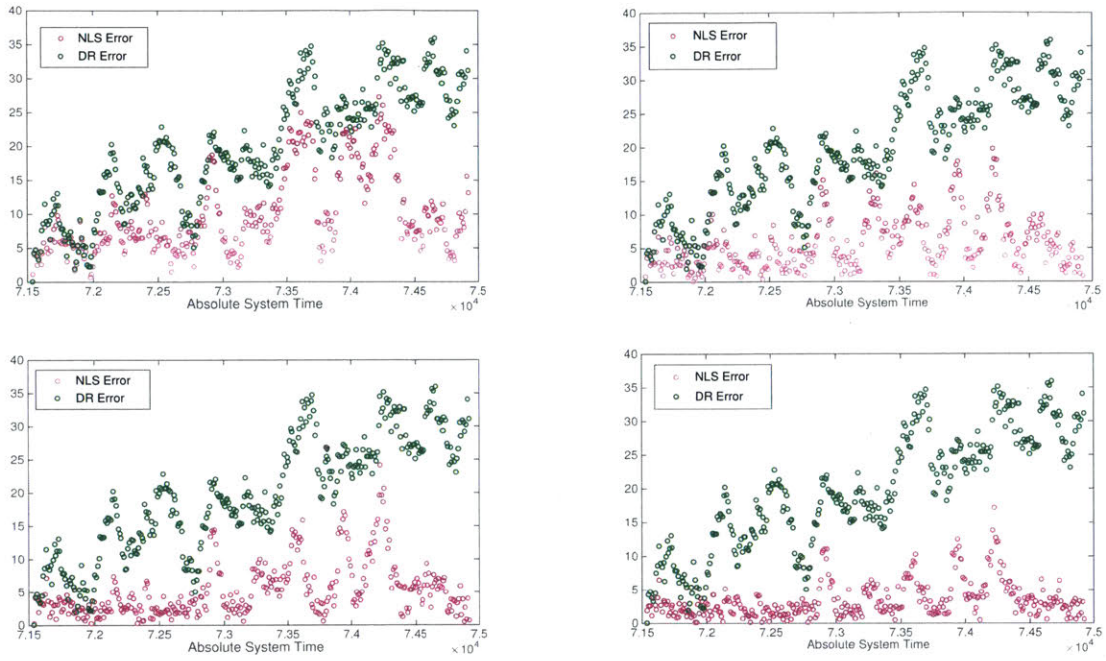

Figure 3-12: Error of current position estimate, using RTK-measured trajectory as ground truth, of both the DR trajectory estimate and the maximum likelihood trajectory estimate for all four success cases. Top left: 30% measurements used. Top right: 50% measurements used. Bottom left: 70% of measurements used. Bottom right: 90% of measurements used.

performance to the Gauss-Newton method far away from the local minimum.

The Levenberg-Marquardt method takes advantage of these two methods by iteratively recomputing an algorithmic parameter, which determines whether the algorithm makes a gradient descent state estimate update or a Gauss-Newton state estimate update. [38]

3.4 Summary

This chapter has presented the formulation of the nonlinear least squares optimization problem for computing the maximum likelihood estimate of the trajectory of a vehicle or multiple vehicles using a combination of measurements. The formulation, including the state description and the observation models, has been presented for a three particular experimental topographies: the configuration in which one GPS-

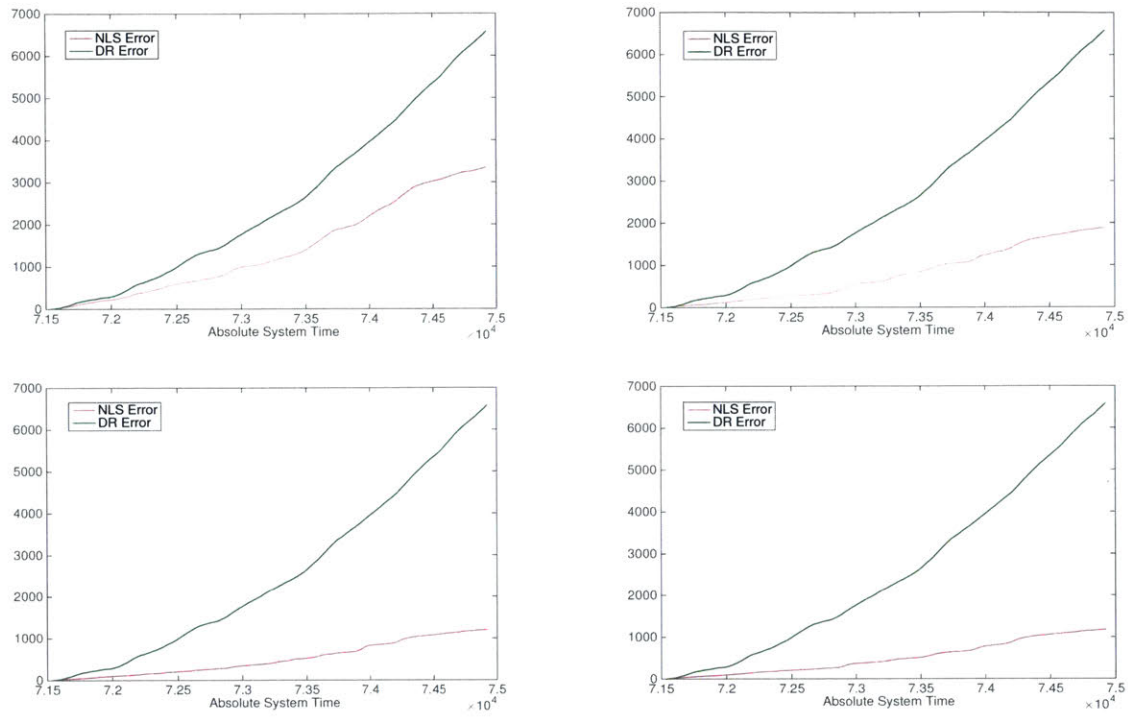

Figure 3-13: Cumulative error of current position estimate, using RTK-measured trajectory as ground truth, of both the DR trajectory estimate and the maximum likelihood trajectory estimate for all four success cases. Top left: 30% measurements used. Top right: 50% measurements used. Bottom left: 70% of measurements used. Bottom right: 90% of measurements used.

aided CNA assists two client nodes, the configuration in which three vehicles each have an initial GPS-measurement, then only inter-vehicle ranges and odometry measurements thereafter, and finally the configuration in which two GPS-aided CNAs assist one client node. By introducing measurement dropouts, it was shown that greater packet transmission success rates induce more accurate NLS trajectory estimates. The following chapter describes an actual mission carried out on the Charles River in Cambridge, MA, and how data from that mission was used to estimate the trajectory of one vehicle as in the third configuration described in this chapter.

Chapter 4

Experimental Results

In this chapter, treatment of data from a mission conducted on the Charles River in Cambridge, MA on November 26, 2014 is described. The quality of the data from the mission is briefly described through analysis of the error in the OWTT-derived range information, and the error analysis is used to determine a superior estimate of the speed of sound in the water during the mission for use in converting the OWTT measurements to range measurements. Following that, the NLS trajectory estimate is computed for one client node vehicle using range measurements to two GPS-aided CNAs in two cases: firstly using the range measurements for both partially and completely successfully received acoustic packets, and secondly using the range measurements only when an acoustic packet is completely successfully received.

4.1 Experimental Setup

Both experiments described in this work utilized autonomous kayaks outfitted with computers in a frontseat-backseat configuration. Vehicle commands, including thruster commands, for example, are handled by the frontseat computer, while custom applications of a vehicle's MOOS community are run on the backseat computer. Furthermore, each vehicle is outfitted with a Woods Hole Oceanographic Institute Micromodem, shown in Figure 4-1, which receives and transmits acoustic packets.

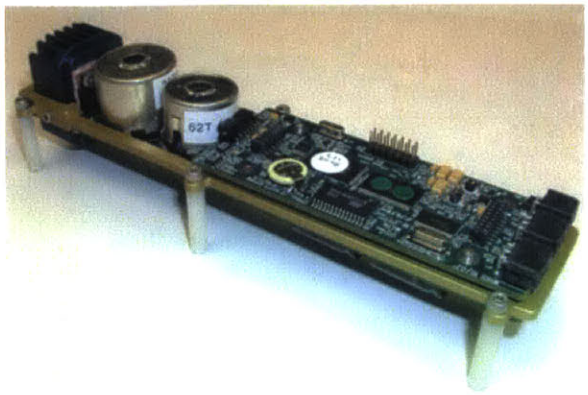

Figure 4-1: The WHOI Micro-Modem.

4.2 Error Analysis on Previous Mission Data

On November 26th, 2014, a simple mission was executed, in which three autonomous kayaks, Kestrel, Nostromo and Silvana, each followed a lawnmower path by approaching predetermined waypoints, while broadcasting acoustic packets in turn. The three vehicles during this mission are shown in Figure 4-2.

Upon completion or termination of a mission, a number of log files are generated for each vehicle. For this error analysis, we use the asynchronous mission log (alog) file of each of the three vehicles; the asynchronous log file gives all values of all variables throughout a mission. Using the alogParse tool written by Josh Leighton, it was possible to get values for desired variables only at times at which chosen variables were updated from the unwieldy alog files. The following variables were thus extracted from each vehicle's alog file at each time at which the variable SYSTEM_TIME_SECONDS was updated:

- SYSTEM_TIME_SECONDS, which is the mission timestamp, synchronized across the entire vehicle network.

- ACOMMS_ONE_WAY_TRAVEL_TIME, which indicates the time taken for the acoustic packet to reach a vehicle after being broadcast by another vehicle.

- ACOMMS_RECEIVED_STATUS, which can take the value of 0, 1 or 2. A value of 0 indicates that all frames of the packet were successfully received. A

Figure 4-2: Autonomous kayaks on the Charles River in Cambridge, MA during mission on November 26, 2015.

value of 1 indicates that only some of the frames of a packet were received. A value of 2 indicates that none of the packet was successfully received. In the case in which none of the frames of a packet are successfully received, we still obtain the one way travel time of the acoustic signal.

- RTK_X & RTK_Y, the real time kinematic (RTK) satellite navigation x- and y-coordinate measurements, which were used as the vehicle's ground truth position on the surface of water. Throughout this thesis, the RTK data is treated as GPS data.

- ACOMMS_SOURCE_ID, which is the ID of the vehicle that broadcast the received acoustic packet. For this mission, Silvana had ID 2, Nostromo had ID 3, and Kestrel had ID 4. For failed acoustic packet, it was not possible for the system to determine which vehicle broadcast the received acoustic packet; in this case, the ACOMMS_SOURCE_ID holds the value of -1.

Indicators for received packet success superimposed on the GPS-measured trajectory of each vehicle are shown in Figures 4-3, 4-4 and 4-5: all frames successfully

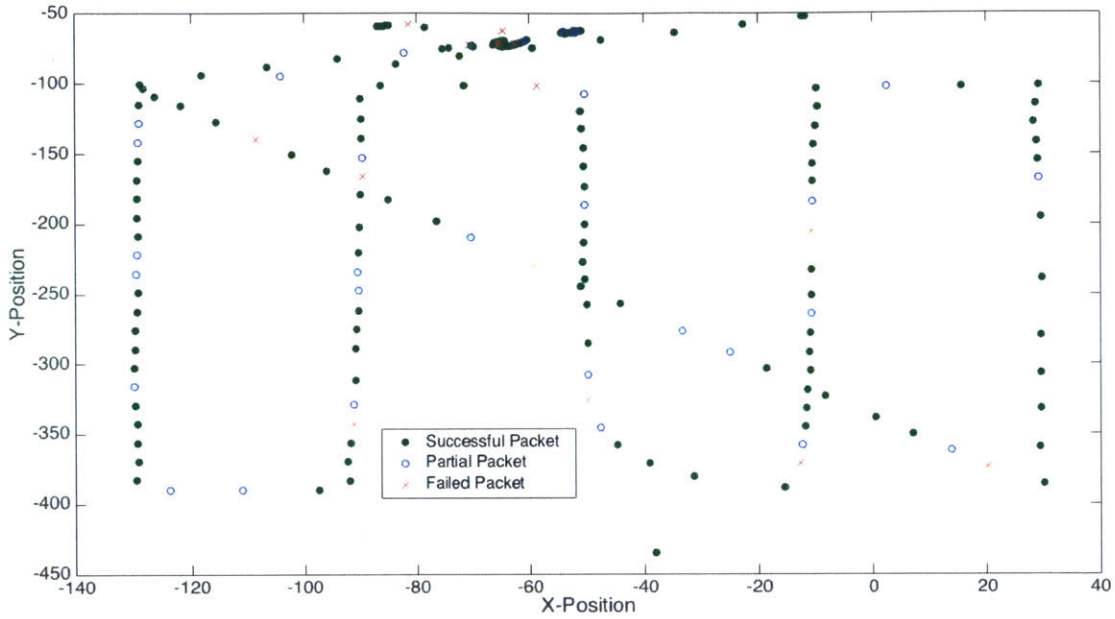

Figure 4-3: Packet success indicators overlaid on Kestrel's GPS-measured trajectory during November 26th, 2014 mission.

Vehicle Name	Kestrel	Nostromo	Silvana
Completely Successful (%)	75	69	72
Partially Successful (%)	18	22	20
Completely Unsuccessful (%)	7	9	8

Table 4.1: Percentage of received packets which were completely successfully received, partially successfully received, or completely unsuccessfully received.

received (green shaded circle), frames of packet partially successfully received (blue unshaded circle), or all packets failed (red cross). Table 4.1 shows the percentage of all packets to be received which were completely successful, partially successful or completely unsuccessful for each vehicle.

This data highlights the issue with discarding partially successfully received packets. If the information encoded in these partially successfully received packets can be used, that increases the number of packets used from approximately 70% to approximately 90%. In increasing the number of range measurements, there should be an improvement in the accuracy of the trajectory estimate of a vehicle.

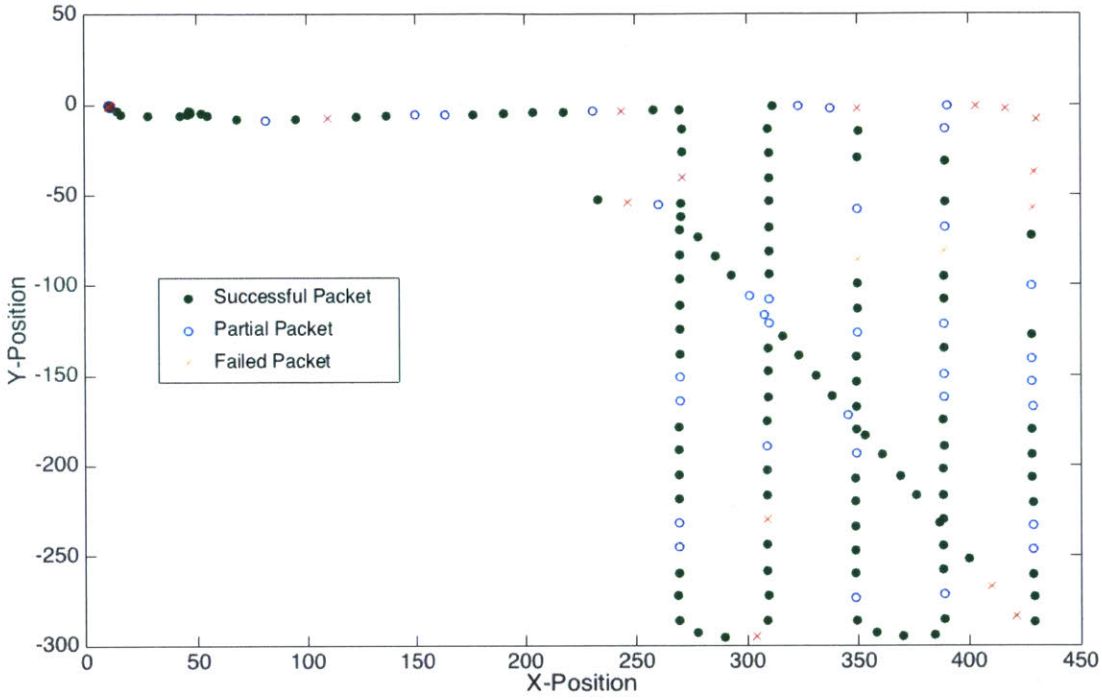

Figure 4-4: Packet success indicators overlaid on Nostromo's GPS-measured trajectory during November 26th, 2014 mission.

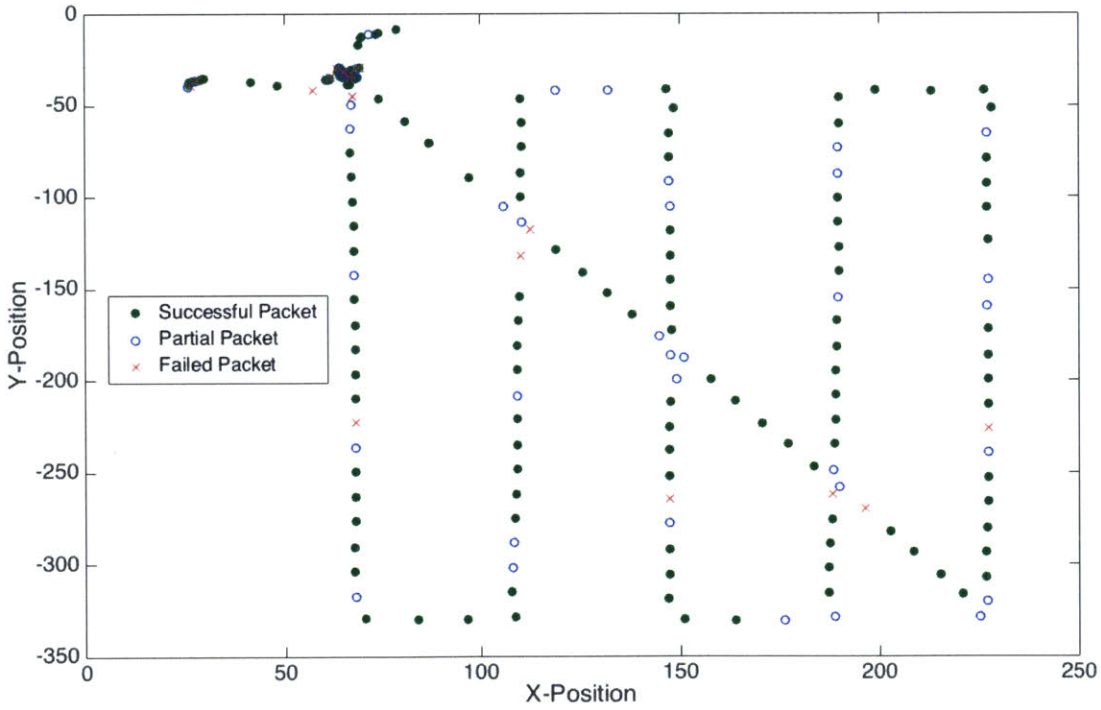

Figure 4-5: Packet success indicators overlaid on Silvana's GPS-measured trajectory during November 26th, 2014 mission.

4.3 Using Error Analysis Results to Compute the Speed of Sound

The speed of sound in water is dependent on a number of physical properties: temperature, salinity and depth. While pressure and salinity increase linearly with depth, the relationship between temperature and depth is nonlinear. As a result, the depth profile of the speed of sound in the open ocean also nonlinear. This relationship was characterized in 1981 by Mackenzie, who presented an empirical equation and the following coefficients for the speed of sound, c, in meters per second, in water as a function of temperature,T, in degrees Celsius, salinity, S, in parts per thousand, and depth, z, in meters [39].

$$c = a_1 + a_2T + a_3T^2 + a_4T^3 + a_5(S-35) + a_6z + a_7z^2 + a_8T(S-35) + a_9Tz^3 \quad (4.1)$$

$$a_1 = 1448.96 \qquad a_2 = 4.591 \qquad a_3 = -5.304 \times 10^{-2}$$

$$a_4 = 2.374 \times 10^{-4} \qquad a_5 = 1.340 \qquad a_6 = 1.630 \times 10^{-2}$$

$$a_7 = 1.675 \times 10^{-7} \qquad a_8 = -1.025 \times 10^{-2} \qquad a_9 = -7.139 \times 10^{-13}$$

As is evident from the above equation, the speed of sound can vary significantly throughout the course of a mission, especially over long distances in the open ocean. In the experiments conducted on the Charles River described here, however, it may be assumed that the speed of sound remained approximately constant over the course of each mission, which was only a few hours long, and it may also be assumed that the acoustic modems remained at approximately the same depth. Without conductivity, temperature and actual depth (CTD) measurements, however, this equation could not be used to determine the correct speed of sound.

Error in the speed of sound used to compute the inter-vehicle range measurements

using the the one-way travel times of acoustic signals introduces systematic error into the data. The equations below shows that the error introduced in the speed of sound estimate is directly proportional to the error in the OWTT-derived range measurement. The true speed of sound in water during the mission is denoted as v_{SW}, the error in the speed of sound is denoted as ϵ, the true distance traveled by the acoustic signal is r, and the computed distance traveled using the incorrect speed of sound, v'_{SW}, is r'.

$$
\begin{aligned}
r' &= v'_{SW} \cdot OWTT \\
r + \epsilon_r &= (v_{SW} + \epsilon_v) \cdot OWTT \\
r + \epsilon_r &= v_{SW} \cdot OWTT + \epsilon_v \cdot OWTT \\
\epsilon_r &= \epsilon_v \cdot OWTT \\
\epsilon_r &= \frac{\epsilon_v}{v_{SW}} \cdot r
\end{aligned}
$$

If the error in the speed of sound is zero and the assumption of zero-mean, normally-distributed measurement noise holds, the linear regression of the scatter plot data of error in range versus inter-vehicular range should have a gradient of zero. Figure 4-6 shows the scatter plot of the data using the usual estimate of 1500 m/s for the speed of sound. The non-zero gradient of the linear regression indicates that that estimate is incorrect, but in using 1500 m/s as a starting estimate of the speed of sound, the method described in algorithm 1, not unlike the proportional control algorithm, could be used to converge on the correct speed of sound during the mission.

Algorithm 1 Converging on speed of sound, v_{est}, in water during mission

1: $v_{prev} \leftarrow$ initial guess for speed of sound
2: $data \leftarrow$ error in acoustically measured inter-vehicular range vs. true range
3: **while** $g > TOL$ **do** ▷ some predetermined stopping point
4: $\quad v_{est} \leftarrow v_{prev} - g$
5: $\quad g \leftarrow$ gradient of linear regression of $data$ using new v_{est}
6: $\quad v_{prev} \leftarrow v_{est}$
7: **end while**

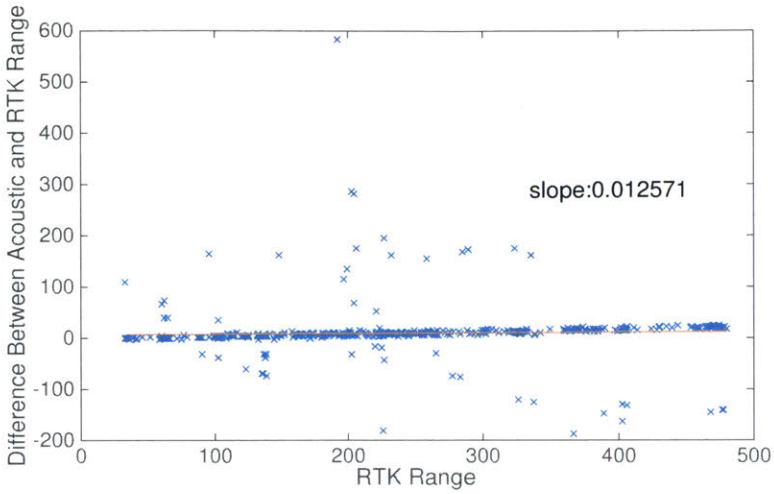

Figure 4-6: Linear regression of range error versus GPS-measured inter-vehicle range using an speed of sound estimate of 1500 m/s.

In another method, the gradient of the linear regression could also be plotted against speed of sound, and the speed of sound corresponding with a zero gradient could be estimated via interpolation. The latter method was used, and the resulting plot is shown in Figure 4-7. Using this method, the speed of sound during the mission was found to be approximately 1481 m/s.

4.4 NLS Optimization Results Using Mission Data

In this mission, vehicles broadcasted acoustic signals in turn. Therefore, at any given time step, a client node would receive a signal from one of the CNAs or neither CNA. A schematic showing the pose graph of this problem is shown below in Figure 4-8.

Using the data from this mission, the maximum likelihood trajectory of one client node vehicle was estimated using its range measurements to the other two vehicles (the GPS-aided CNAs). For each time at which a new packet was received, the GPS-measured position of the sender at send time (computed by subtracting the one-way travel time of the packet from the packet reception time) was found via linear interpolation of the sender's GPS and time data. NLS optimization was used on the resulting maximum likelihood function to obtain the most likely positions of the vehicle (client node) over the course of the mission at times of message reception.

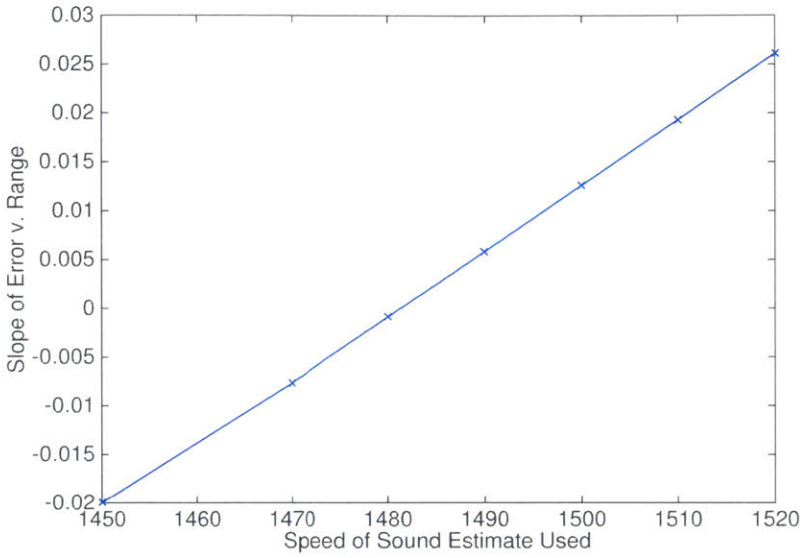

Figure 4-7: Gradient of the linear regression of the range error vs. true range plot for a number of estimates for speed of sound.

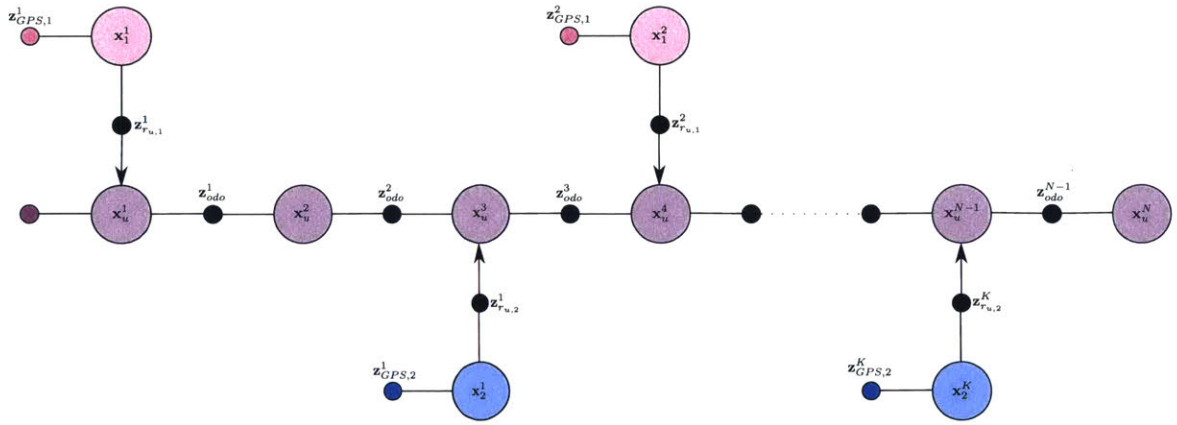

Figure 4-8: Pose graph of the problem, in which a client node vehicle is assisted by two GPS-aided CNAs. In this case, vehicles broadcast information in turn, so at any given time, the client node vehicle may gain information from either one CNA or neither CNA. The CNAs have constant access to GPS measurements. The client node vehicle has access to an initial GPS measurement of its position, its own odometry measurements, and intermittent range-only measurements to the GPS-aided CNAs.

The initial state estimate used in the optimization problem was taken to be the GPS measured positions of the sender vehicles and the dead-reckoned trajectory estimate of the client node vehicle. The cases for the two sets of results are described below.

Case 1 Range-only measurements to and RTK-measurements of the CNAs were only used if the packet was completely successfully received.

Case 2 Range-only measurements to and RTK-measurements of the CNAs were used if the packet was completely or partially successfully received.

Figure 4-9 shows the results of the maximum likelihood trajectory estimation problem for the two cases. The improvement in accuracy of the trajectory estimate in the case in which RTK measurements of both partially received and totally received packets are used can be seen, but is more apparent in the error and cumulative error plots shown in Figures 4-10 and 4-11, respectively. At the end of the mission, the cumulative error in the trajectory estimate in the case in which measurements were used only at times at which complete packets were received was 44% higher than in the case in which measurements from both partially and totally received packets were used.

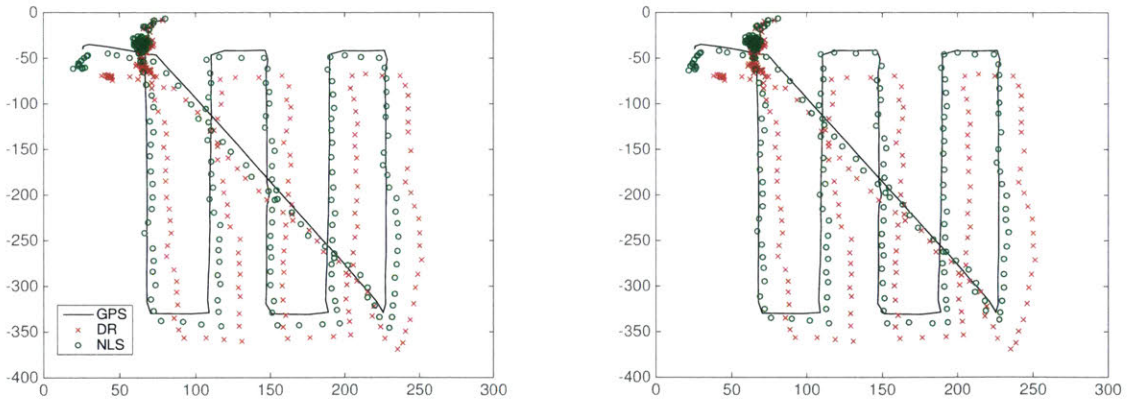

Figure 4-9: RTK-measured ground truth, the dead-reckoned trajectory estimate, and the Levenberg-Marquardt method-computed maximum likelihood trajectory estimate of the vehicle, Silvana, for two cases: using only completely received packets (left) and using both completely and partially received packets (right).

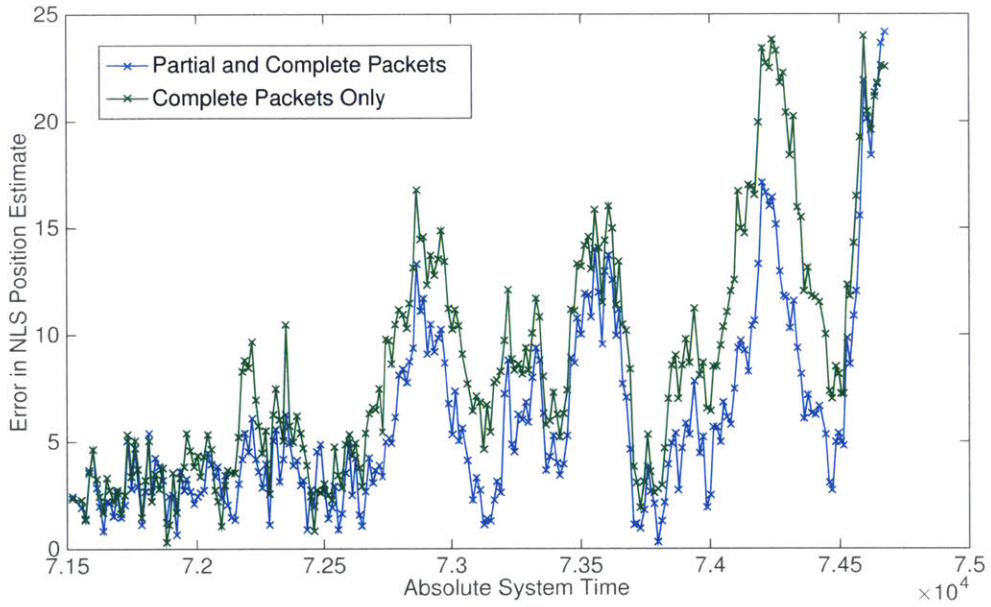

Figure 4-10: The error in the Levenberg-Marquardt method-computed maximum likelihood trajectory estimate of the vehicle, Silvana, using the RTK-measured position as ground truth over the course of the mission for two cases: using only completely received packets (green) and using both completely and partially received packets (blue).

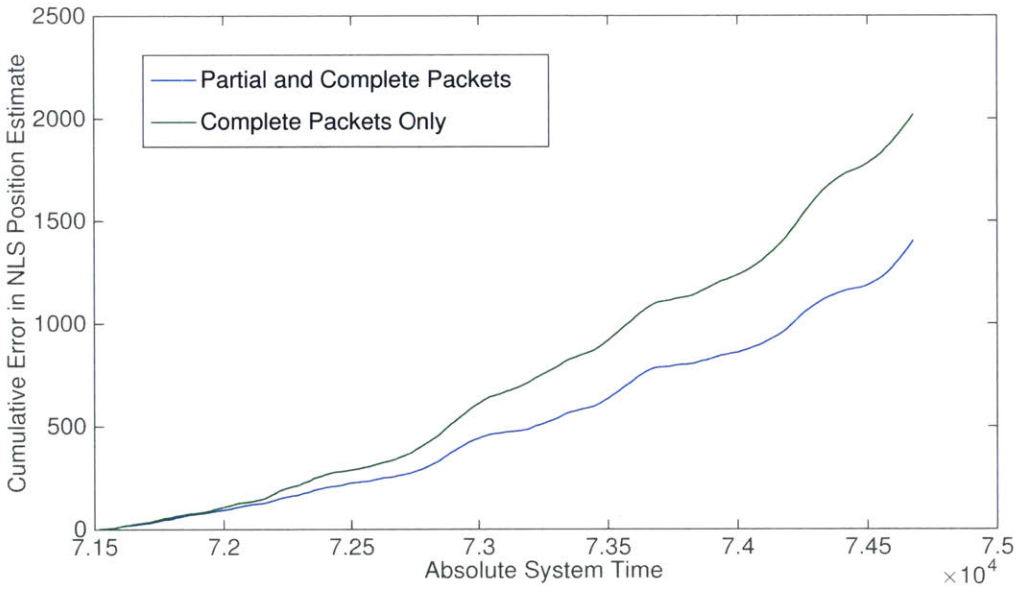

Figure 4-11: The cumulative error in the Levenberg-Marquardt method-computed maximum likelihood trajectory estimate of the vehicle, Silvana, using the RTK-measured position as ground truth over the course of the mission for two cases: using only completely received packets (green) and using both completely and partially received packets (blue).

4.5 Summary

In this chapter, the results of the NLS optimization of the trajectory of a vehicle with the assistance of two CNAs were presented for two cases: one in which range and GPS-derived pose information was used if packets were either partially successful or completely successful, and one in which that information was only used if a packet was completely successfully received. The results showed that the NLS trajectory estimate was superior over the course of the mission in the case in which both sets of packets could be used. In being able to use information from packets, even when partially received, the navigation estimate onboard a vehicle in a decentralized configuration becomes more accurate. Furthermore, in this decentralized configuration, each vehicle will maintain a higher resolution estimate of other vehicles' trajectories, which in turn results in improved behavior in cooperative tasks, such as cooperative area coverage. The results in this chapter justify the implementation of a method of improving the robustness to partial packet loss, which is introduced and described in the following chapter.

Chapter 5

Partial Packet Loss-Aware Cooperative Localization

The work thus far in this thesis has shown that using an increased number of range measurements to GPS-aided CNAs results in a more accurate NLS estimate of that vehicle's trajectory. In this chapter, a method of improving robustness to partial packet loss is introduced. In this method, packets are organized such that in each frame of the packet, there is low resolution spatial information about the trajectory of the transmitting vehicle, so that regardless of the number of frames received by a target, some information about the transmitting vehicle's trajectory may be used to bolster the receiving vehicle's onboard factor graph, and therefore improve the accuracy of its trajectory estimate. This low resolution spatial information is generated using Smith and Cheeseman's method of spatial relationship compounding, and on the receiver's end, the inverse process of decompounding is used to recover binary factors to append to the receiving vehicle's version of the transmitting vehicle's factor graph. The details of this method are described in this chapter.

5.1 Acoustic Transmission of Navigation Information

The WHOI Micromodem uses frequency modulation, a method of varying the instantaneous frequency of a carrier wave, to encode the information to be transmitted in acoustic carrier waves using one of two schemes: the frequency-shift keying (FSK) scheme or the phase-shift keying (PSK) scheme. When FSK is used, data is transmitted by shifting the frequency of the carrier wave across a predefined set of frequencies. When PSK is used, data is transmitted by changing the phase of the carrier wave. As an example, given a set of binary digits, 1s would be transmitted at frequency, f_1 whereas 0s would be transmitted at frequency, f_2 in the FSK scheme. In the PSK scheme, 1s could be transmitted with a zero-degree phase and 0s could be transmitted with a 180-degree phase.

While the FSK scheme is more effective when it comes to noise rejection, the PSK scheme uses the available bandwidth more efficiently, that is, it allows for higher data rates. In fact, of the seven data rates available with the WHOI Micromodem, six use the PSK scheme; in each of these six data rates, each acoustic packet is sent as a collection of n frames, where the total number of bytes transmitted is the product of the frame size and the number of frames, n. In the mission described in Chapter 4, the Rate 1 was used, in which there were three frames per acoustic packet transmitted.

In that mission, it was noted that of all the acoustic messages intended for the client node vehicle, approximately 70% were completely successfully received, approximately 20% were only partially received and approximately 10% were never received, even in part. If range-information to and GPS-measurements of the CNAs could be used by the client node vehicle both when packets were completely successfully received or partially received, then 90% of the packets received could result in measurements used to augment the NLS problem, which would, as shown chapters 3 and 4, result in a more accurate result in the trajectory estimate of the receiving vehicle.

In current methods, odometry information about a transmitting vehicle is sent in

a packet as a sequence of binary odometry factors, each of which is relative to its precursor; although the first odometry factor in the packet may be relative to some origin or contact point known over the network, the odometry factors thereafter are relative to other poses in the packet. Therefore, if a packet is only partially received, odometry measurements are received without information about the pose to which they are relative. The information contained in the packet, as a result, cannot be used to augment the receiving vehicle's factor graph, so it must discarded. This problem can be circumvented by implementing the concept introduced by Walls et al. in their presentation of the origin state method [28], previously discussed in chapter 2 of this thesis. By transmitting each odometry measurement so that it is relative to the network's global origin, and not relative to other poses represented in the acoustic packet, each odometry measurement can independently be used to add information to the receiver's factor graph.

5.2 Designing Custom Packets for Robustness to Partial Packet Loss

Odometry measurements may be described as spatial relationships since they describe the motion undergone by a vehicle to get from one pose to another. Each binary odometry measurement factor connecting two successive poses of a vehicle is relative to the frame of the vehicle in its earlier pose of the two. Two successive odometry measurements, or spatial relationships, may be combined using factor composition or spatial compounding, a process which was first described in 1990 by Smith, Self and Cheeseman [40]. An intermediate pose, x_j, between two poses, x_i and x_k, may thus be marginalized out to obtain the composed odometry measurement, z_{ik}. Thusly, a series of odometry measurements can be compounded to yield a single, exact odometry measurement relative to an origin state. The work described in this thesis takes the state-of-the-art method of robustly sharing odometry measurements relative to an origin state over a network of vehicles, and applies the same concept to enabling

robustness to partial packet loss.

As an example, the schematic in Figure 5-1 shows how four successive odometry measurements would be packed into separate frames for the case in which an acoustic packet is made up of three frames.

Instead of taking the four odometry measurements of the full "message" to be broadcast and packing them in sequence into frames, each odometry measurement is reworked so that it is relative to the origin state, then each reworked odometry measurement is packed into separate frames of the packet, such that they can independently provide useful odometry information to the receiver of the data. For example, if frames 1 and 3 are lost in transmission and only frame 2 of the packet is received by another vehicle, z_{Oj} and z_{jl} can be recovered by the receiving vehicle through decompounding and that information can then be incorporated into that vehicle's factor graph of the vehicle network.

A sequence of odometry measurements can be compounded as described in Algorithm 2. The method of preparing acoustic packets on the sender side, so that each frame consists of an odometry measurement relative to the origin state, is outlined in Algorithm 3, and the method of recovering an odometry measurement on the receiver side using decompounding is described in Algorithm 4. Details of the process of compounding and decompounding odometry factors are presented in the following section.

Algorithm 2 Compound a time-ordered vector of odometry measurements

```
1: procedure COMPOUND(odometries)
2:     l ← length of odometries
3:     result ← odometries(1)
4:     for i ← 2, l do
5:         result ← result ⊕ odometries(i)
6:     end for
7:     return result
8: end procedure
```

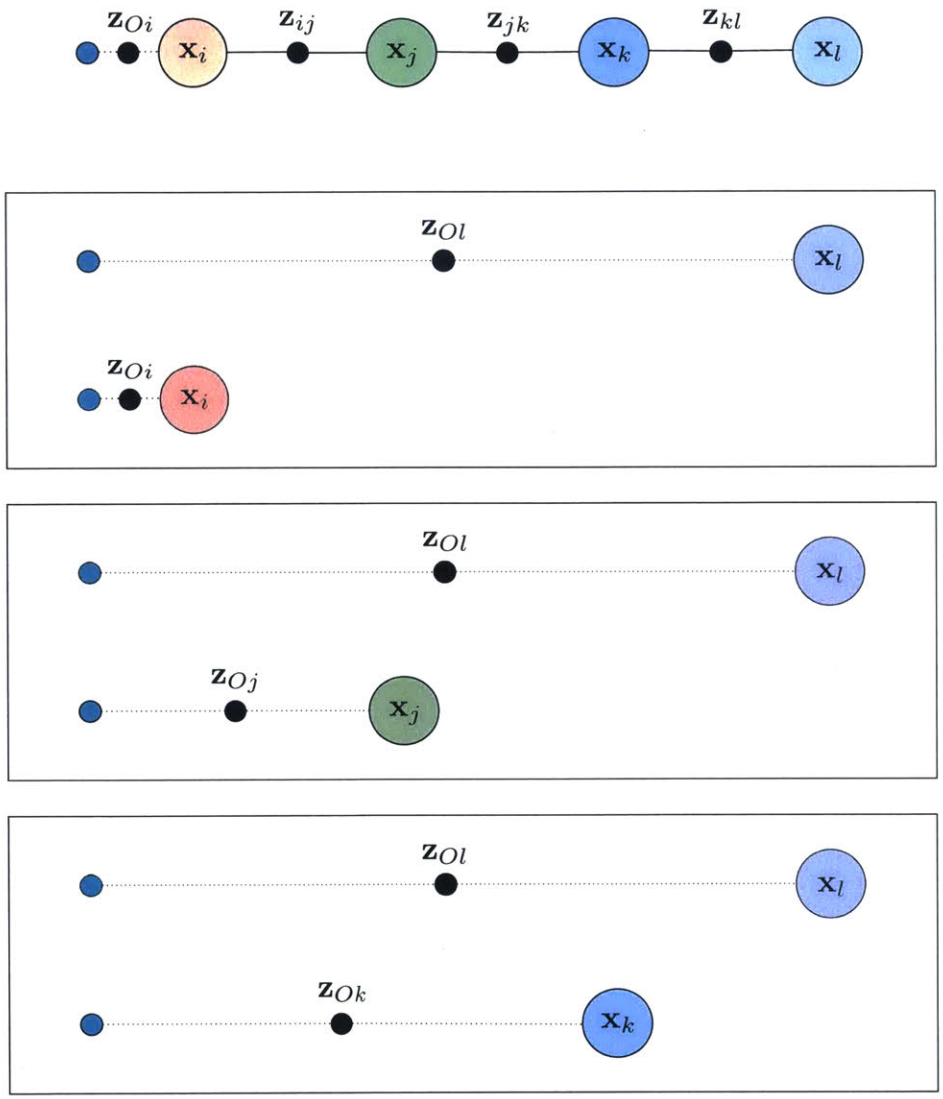

Figure 5-1: Schematic showing how compounded odometry measurements would be packed into three separate frames, enabling robustness to partial packet loss. Each frame of this packet is independently useful to a receiver.

Algorithm 3 Packing acoustic packets for partial packet loss-aware cooperative navigation

Ensure: *timestamps* and *odometries* are of the same length

timestamps ← all own-ship timestamps, time-ordered
odometries ← all own-ship odometry measurements, time-ordered
$frames$ ← frames of packet to be transmitted
l ← length of *odometries*
n ← number of frames per packet
for $i \leftarrow 1, n$ **do**
    $compoundedTime \leftarrow \text{COMPOUND}(timestamps(1 : l - n + i))$
    $compoundedOdometries \leftarrow \text{COMPOUND}(odometries(1 : l - n + i))$
    add $compoundedTime$ **to** $frames(i)$
    add $compoundedOdometries$ **to** $frames(i)$
    while $frames(i)$ is not full **do**
        add "filler" bits to $frames(i)$
    end while
end for

Algorithm 4 Recovering odometry measurements from received compounded measurements

Ensure: received frames are time-ordered

odometries ← all odometry measurements previously received from sender
state ← COMPOUND(*odometries*)
n ← number of received frames
for $i \leftarrow 1, n$ **do**
    $newMeasurement \leftarrow compoundedOdometries$ from $frames(i)$
    $newOdometry \leftarrow \ominus state \oplus newMeasurement$
    append $newOdometry$ **to** *odometries*
end for

5.3 Spatial Relationship Composition & Decomposition

Throughout this work, all motion is assumed to be planar. Thus, a vehicle's pose is described by its coordinates in a two-dimensional Cartesian frame, x and y, and its orientation, ϕ, the rotation about the z-axis. Vehicles lie on the surface of the water, and the z-axis points downwards, aligning with gravity. The pose of a vehicle is denoted as $\mathbf{x}$; the pose may also be described as a spatial variable. The spatial relationship between two poses $\mathbf{x}_i$ and $\mathbf{x}_j$ is $\mathbf{x}_{ij}$, and it represents the spatial change in the vehicle's pose, reference from the body frame of the vehicle when it holds pose $\mathbf{x}_i$. The odometry measurement of this spatial change is denoted as $\mathbf{z}_{ij}$.

The compounding of two odometry measurements, $\mathbf{z}_{ij}$ and $\mathbf{z}_{jk}$ to obtain compounded odometry measurement $\mathbf{z}_{ik}$ is denoted as

$$\mathbf{z}_{ik} = \mathbf{z}_{ij} \oplus \mathbf{z}_{jk} \tag{5.1}$$

The odometry measurement $\mathbf{z}_{ij}$ denotes the measurement of the change in the vehicle's pose from $\mathbf{x}_i$ to $\mathbf{x}_j$, measured in the body frame of the vehicle when it holds pose, $\mathbf{x}_i$. Similarly, the odometry measurement $\mathbf{z}_{jk}$ denotes the measurement of the change in the vehicle's pose from $\mathbf{x}_j$ to $\mathbf{x}_k$, measured in the body frame of the vehicle when it holds pose, $\mathbf{x}_j$. Because the two measurements being composed are in two different frames, the composition does not trivially reduce to addition. The measurement, $\mathbf{z}_{jk}$ must be converted to the frame of the vehicle when it holds pose, $\mathbf{z}_i$, if addition is to be used to obtain the compounded measurement $\mathbf{z}_{ik}$, that is, the change in the vehicle's pose from $\mathbf{x}_i$ to $\mathbf{x}_k$, measured in the body frame of the vehicle when it holds pose, $\mathbf{x}_i$.

The odometry measurement, $\mathbf{z}_{jk}$ converted to the frame of the vehicle when it holds pose, $\mathbf{z}_i$, is

$$\begin{bmatrix} x_{jk}\cos\phi_{ij} - y_{jk}\sin\phi_{ij} \\ x_{jk}\sin\phi_{ij} - y_{jk}\cos\phi_{ij} \\ \phi_{jk} \end{bmatrix}$$

Thus, the compounded odometry measurement is computed as

$$\mathbf{z}_{ik} = \begin{bmatrix} x_{ij} + x_{jk}\cos\phi_{ij} - y_{jk}\sin\phi_{ij} \\ y_{ij} + x_{jk}\sin\phi_{ij} - y_{jk}\cos\phi_{ij} \\ \phi ij + \phi_{jk} \end{bmatrix} \tag{5.2}$$

Once a vehicle receives two compounded odometry measurements, the inverse process, decomposition, may then be implemented to recover the odometry factor composed to produce the low resolution spatial relationship prior to transmission. The inverse process of composition is denoted as

$$\mathbf{z}_{ji} = \ominus \mathbf{z}_{ij} \tag{5.3}$$

Given the odometry measurement when the vehicle transitions from pose $\mathbf{x}_i$ to pose $\mathbf{x}_j$, $\mathbf{z}_{ij}$, the odometry measurement that should result when the vehicle transitions from $\mathbf{x}_j$ to $\mathbf{x}_i$, $\mathbf{z}_{ji}$, in the frame of the vehicle as it hold pose $\mathbf{x}_j$ is computed as

$$\mathbf{z}_{ji} = \begin{bmatrix} -z_{ij}\cos\phi_{ij} - y_{ij}\sin\phi_{ij} \\ x_{ij}\sin\phi_{ij} - y_{ij}\cos\phi_{ij} \\ -\phi ij \end{bmatrix} \tag{5.4}$$

The process for recovering the odometry measurement, $\mathbf{z}_{jk}$, from the odometry measurement, $\mathbf{z}_{ij}$, and the compounded odometry measurement, $\mathbf{z}_{ik}$, is therefore

$$\mathbf{z}_{jk} = \mathbf{z}_{ji} \oplus \mathbf{z}_{ik} \tag{5.5}$$

$$\mathbf{z}_{jk} = \ominus \mathbf{z}_{ij} \oplus \mathbf{z}_{ik} \tag{5.6}$$

5.4 Summary

In this chapter, a method of partial packet loss-aware cooperative navigation was proposed. By compounding all odometry measurements so that they are relative to a network-wide origin state then packing them into individual frames of a packet, loss of some number of frames of a packet no longer renders a packet unsuable, since the frames become independently useful. Regardless of the number of frames of a packet received, decompounding can be used on the receiver end to recover the odometry measurement encoded in each received frame. Due to time constraints, it was not possible to fully implement this method, and full implementation in both simulation and field experiments remains an area for future research. Areas for future research and a summary of the work presented in this thesis are stated in the following chapter.

Chapter 6

Summary and Future Work

6.1 Thesis Summary

This thesis described the process of computing the maximum likelihood trajectory estimate of a vehicle in a number of CNA-client node configurations. For the configuration in which two CNAs assist one client node without access to its own global positioning estimate, it was shown that the number of range measurements between the CNAs and the client node correlates with the accuracy of the resulting NLS trajectory estimate of the client node. This result was used to hypothesize that if a client node could use measurements associated with both completely successfully and partially successfully received packets, instead of only those associated with completely successfully received packets, a more accurate trajectory estimate would result. Data from field experiments conducted using three autonomous kayaks equipped with an acoustic communications system was used to verify this hypothesis. Finally, a method was proposed to allow for the use of partially received packets; by utilizing spatial relationship compounding, poses can be expressed relative to a network-wide origin state, and by packing compounded odometry measurements into individual frames, odometry measurements can be recovered from the resulting independently useful frames through the inverse process of spatial relationship decompounding.

6.2 Proposed Future Work

In this thesis, all computation was carried out by solving the maximum-likelihood estimation problem using the collection of proprioceptive measurements and range measurements to GPS-aided CNAs in post-processing. For many missions, it is much more useful to have an acceptable estimate of a vehicle's position during the course of a mission, so in future work, it would be preferable to implement an online estimator, such as the incremental smoothing and mapping (iSAM) algorithm, which would provide a continuous estimate of a vehicle's state in the field throughout a mission. Implementation of this proposed method of partial packet loss-aware cooperative navigation, using the proposed method of odometry compounding to generate independently useful frames, in simulation then eventually in field experiments remains an area for future research.

Bibliography

[1] S.L. Walker, C. E. de Ronde, D. J. Fornari, M. I. Leybourne, V. Ferrini, R. Littlefield A. Kukulya, B. J. Scott, D. Immenga, and E. T. Baker. Hydrothermal Venting at Lake Rotomahana, New Zealand, 125 Years After the Tarawera Eruption of 1886. In *AGU Fall Meeting Abstracts*, volume 1, page 0840, 2011.

[2] K. W. Nicholls, E. P. Abrahamsen, J. J. H. Buck, P. A. Dodd, C. Goldblatt, G. Griffiths, and K. J. Heywood. Measurements beneath an Antarctic ice shelf using an autonomous underwater vehicle. *Geophysical Research Letters*, 33(8), April 2006.

[3] Clayton Kunz, Chris Murphy, Hanumant Singh, Claire Pontbriand, Robert A. Sohn, Sandipa Singh, Taichi Sato, Chris Roman, Ko-ichi Nakamura, Michael Jakuba, Ryan Eustice, Richard Camilli, and John Bailey. Toward extraplanetary under-ice exploration: Robotic steps in the Arctic. *Journal of Field Robotics*, 26(4):411–429, 2009.

[4] Marcia McNutt. The hunt for MH370. *Science*, 344(6187):947–947, 2014.

[5] Ya-Wen Huang, Yuki Sasaki, Yukihiro Harakawa, Edwardo F. Fukushima, and Shigeo Hirose. Operation of underwater rescue Robot anchor diver III during the 2011 Tohoku earthquake and tsunami. In *OCEANS 2011*, pages 1–6, 2011.

[6] Richard Camilli, Christopher M. Reddy, Dana R. Yoerger, Benjamin AS Van Mooy, Michael V. Jakuba, James C. Kinsey, Cameron P. McIntyre, Sean P. Sylva, and James V. Maloney. Tracking hydrocarbon plume transport and biodegradation at Deepwater Horizon. *Science*, 330(6001):201–204, 2010.

[7] Yanwu Zhang, Robert S. McEwen, John P. Ryan, James G. Bellingham, Hans Thomas, Charles H. Thompson, and Erich Rienecker. A peak-capture algorithm used on an autonomous underwater vehicle in the 2010 Gulf of Mexico oil spill response scientific survey. *Journal of Field Robotics*, 28(4):484–496, 2011.

[8] M. F. Fallon, G. Papadopoulos, J. J. Leonard, and N. M. Patrikalakis. Cooperative AUV navigation using a single maneuvering surface craft. *Intl. J. of Robotics Research*, 29(12):1461–1474, October 2010.

[9] J. Vaganay, J.J. Leonard, J.A. Curcio, and J.S. Willcox. Experimental validation of the moving long base-line navigation concept. In *Autonomous Underwater Vehicles, 2004 IEEE/OES*, pages 59–65, Jun. 2004.

[10] Ian F Akyildiz, Dario Pompili, and Tommaso Melodia. Challenges for efficient communication in underwater acoustic sensor networks. *ACM Sigbed Review*, 1(2):3–8, 2004.

[11] Ryan M. Eustice, Hanumant Singh, and Louis L. Whitcomb. Synchronous-clock, one-way-travel-time acoustic navigation for underwater vehicles. *Journal of Field Robotics*, 28(1):121–136, 2011.

[12] M.R. Benjamin, J.J. Leonard, H. Schmidt, and P. Newman. An overview of MOOS-IvP and a users guide to the IvP helm autonomy software - release 4.2.1. Technical Report MIT-CSAIL-TR-2011-037, Computer Science and Artificial Intelligence Laboratory, MIT, August 2011.

[13] Toby Edwin Schneider. *Advances in Integrating Autonomy with Acoustic Communications for Intelligent Networks of Marine Robots.* PhD thesis, Massachusetts Institute of Technology, February 2013.

[14] Andrew Patrikalakis Joseph Curcio, John Leonard. SCOUT-a low cost autonomous surface platform for research in cooperative autonomy. In *OCEANS 2005*, pages 725–729, 2005.

[15] Justin E. Manley. Development of the autonomous surface craft "ACES". In *OCEANS 1997*, volume 2, pages 827–832, 1997.

[16] S. E. Webster, R. M. Eustice, C. Murphy, H. Singh, and L. L. Whitcomb. Toward a platform-independent acoustic communications and navigation system for underwater vehicles. In *Proc. of the IEEE/MTS OCEANS Conf. and Exhibition*, Biloxi, MS, 2009.

[17] R. Eustice, L. Whitcomb, H. Singh, and M. Grund. Recent advances in synchronous-clock one-way-travel-time acoustic navigation. In *Proc. of the IEEE/MTS OCEANS Conf. and Exhibition*, pages 1–6, Boston, MA, USA, 2006.

[18] R. M. Eustice, L. L. Whitcomb, H. Singh, and M. Grund. Experimental results in synchronous-clock one-way-travel-time acoustic navigation for autonomous underwater vehicles. In *IEEE Intl. Conf. on Robotics and Automation (ICRA)*, pages 4257–4264, Rome, Italy, April 2007.

[19] G. Papadopoulos, M.F. Fallon, , J.J. Leonard, and N. M. Patrikalakis. Cooperative localization of marine vehicles using nonlinear state estimation. In *IEEE/RSJ Intl. Conf. on Intelligent Robots and Systems (IROS)*, Taipei, Taiwan, October 2010.

[20] S. E. Webster, R. M. Eustice, H. Singh, and L. L. Whitcomb. Preliminary deep water results in single-beacon one-way-travel-time acoustic navigation for underwater vehicles. In *IEEE/RSJ Intl. Conf. on Intelligent Robots and Systems (IROS)*, 2009.

[21] S. Thrun, W. Burgard, and D. Fox. *Probabilistic Robotics.* The MIT Press, Cambridge, MA, 2005.

[22] S.E. Webster, R.M. Eustice, H. Singh, and L.L. Whitcomb. Advances in single-beacon one-way-travel-time acoustic navigation for underwater vehicles. *The International Journal of Robotics Research*, 2012.

[23] A. Bahr, J.J. Leonard, and M.F. Fallon. Cooperative localization for autonomous underwater vehicles. *Intl. J. of Robotics Research*; 28(6):714–728, 2009.

[24] Jeffrey M. Walls and Ryan M. Eustice. Experimental comparison of synchronous-clock cooperative acoustic navigation algorithms. In *Proceedings of the IEEE/MTS OCEANS Conference and Exhibition*, Kona, HI, USA, September 2011.

[25] S.E. Webster, J.M. Walls, L.L. Whitcomb, and R.M. Eustice. Decentralized extended information filter for single-beacon cooperative acoustic navigation: Theory and experiments. *Robotics, IEEE Transactions on*, 29(4):957–974, Aug 2013.

[26] Sarah E. Webster. *Decentralized single-beacon acoustic navigation: combined communication and navigation for underwater vehicles.* PhD thesis, Johns Hopkins University, Baltimore, MD, USA, June 2010.

[27] Sarah E. Webster, Louis L. Whitcomb, and Ryan M. Eustice. Preliminary results in decentralized estimation for single-beacon acoustic underwater navigation. In *Robotics: Science and Systems (RSS)*, Zaragoza, Spain, June 2010.

[28] Jeffrey M. Walls and Ryan M. Eustice. An origin state method for communication constrained cooperative localization with robustness to packet loss. *The International Journal of Robotics Research*, 33(9):1191–1208, 2014.

[29] Jeffrey M. Walls and Ryan M. Eustice. An exact decentralized cooperative navigation algorithm for acoustically networked underwater vehicles with robustness to faulty communication: Theory and experiment. In *Proceedings of the Robotics: Science & Systems Conference*, Berlin, Germany, June 2013.

[30] A. Bahr, M. Walter, and J.J. Leonard. Consistent cooperative localization. In *IEEE Intl. Conf. on Robotics and Automation (ICRA)*, pages 3415–3422, May 2009.

[31] M. F. Fallon, G. Papadopoulos, and J. J. Leonard. A measurement distribution framework for cooperative navigation using multiple AUVs. In *IEEE Intl. Conf. on Robotics and Automation (ICRA)*, pages 4803–4808, May 2010.

[32] L. Paull, M. Seto, and J. J. Leonard. Decentralized cooperative trajectory estimation for autonomous underwater vehicles. In *IEEE/RSJ Intl. Conf. on Intelligent Robots and Systems (IROS)*, 2014.

[33] Jeffrey M. Walls, Alexander G. Cunningham, and Ryan M. Eustice. Cooperative localization by factor composition over a faulty low-bandwidth communication channel. In *Proceedings of the IEEE International Conference on Robotics and Automation*, 2015.

[34] F. Dellaert and M. Kaess. Square Root SAM: Simultaneous localization and mapping via square root information smoothing. *Intl. J. of Robotics Research*, 25(12):1181–1203, December 2006.

[35] M. Kaess, A. Ranganathan, and F. Dellaert. iSAM: Incremental smoothing and mapping. *Robotics, IEEE Transactions on*, 24(6):1365–1378, Dec. 2008.

[36] D.M. Rosen, M. Kaess, and J.J. Leonard. An incremental trust-region method for robust online sparse least-squares estimation. In *IEEE Intl. Conf. on Robotics and Automation (ICRA)*, pages 1262–1269, St. Paul, MN, May 2012.

[37] Ananth Ranganathan. The Levenberg-Marquardt Algorithm, June 2004.

[38] Henri P. Gavin. The Levenberg-Marquardt method for nonlinear least squares curve-fitting problems, October 2013.

[39] Kenneth V. Mackenzie. Nine-term equation for sound speed in the oceans. *The Journal of the Acoustical Society of America*, 70(3):807–812, 1981.

[40] R. Smith, M. Self, and P. Cheeseman. Autonomous robot vehicles. In Ingemar J. Cox and Gordon T. Wilfong, editors, *Autonomous Robot Vehicles*, chapter Estimating Uncertain Spatial Relationships in Robotics, pages 167–193. Springer-Verlag New York, Inc., New York, NY, USA, 1990.